RESILIENT OPERATION AND OPTIMAL SCHEDULING OF NETWORKED MICROGRIDS

by

Faria Kamal

A dissertation submitted to the faculty of
The University of North Carolina at Charlotte
in partial fulfillment of the requirements
for the degree of Doctor of Philosophy in
Electrical Engineering

Charlotte

2023

Approved by:

Dr. Badrul Chowdhury

Dr. Valentina Cecchi

Dr. Madhav Manjrekar

Dr. Churlzu Lim

ABSTRACT

FARIA KAMAL. Resilient Operation and Optimal Scheduling of Networked Microgrids. (Under the direction of DR. BADRUL CHOWDHURY)

The rapid proliferation and widespread adoption of microgrids (MG) necessitate the development of new methodologies to holistically model all the active components within MGs. It's crucial to focus on specific islanding requirements, especially when the primary grid power is unavailable. In order to ensure a high level of reliability in an interconnected MG network, this dissertation presents an optimal scheduling model designed to minimize the day-ahead costs of the MGs while taking into account the existing operational constraints.

This problem is thoughtfully decomposed using Bender's Decomposition method into two key operating conditions: grid-connected and resilient operations. The ultimate goal is to ensure that each MG within the network maintains sufficient online capacity in the event of an emergency islanding situation, such as during extreme weather events. These events often come with uncertainties regarding their timing and duration, necessitating the consideration of multiple potential islanding scenarios for each event.

The primary objective of this thesis is to establish optimal scheduling that guarantees the feasibility of islanding for all conceivable scenarios of such events, with load shedding as a last resort. The optimization model has been put into practice across different layouts of the modified IEEE 123-bus test system, encompassing various events over a 24-hour period. In addition to proposing a day-ahead scheduling approach oriented towards resiliency for multiple MGs, a comprehensive cost analysis and comparisons among all the test cases are also offered. The results convincingly demonstrate the utility of the proposed day-ahead scheduling algorithm, particularly for MG owners looking to foster collaborations with neighboring MGs. Lastly, after

comparing with the traditional Single Stage MILP approach, the proposed method has proven to be computationally faster for practical usage. It has been shown that decomposing the problem using the proposed model makes it possible to combat real life events with thousand scenarios, where the single stage approach may fail.

DEDICATION

I dedicate this dissertation to the most extraordinary woman in my life, my beloved mother, Hasina Momtaz.

You have been my rock, my confidante, and my source of inspiration. Your sacrifices and support have made this achievement possible, and for that, I am eternally grateful. Your enduring belief in my dreams and your endless encouragement, even during the most challenging times, have been my motivation.

This dissertation stands as a testament to your profound influence on my life and my academic journey. It is dedicated to you, with all my love and gratitude.

ACKNOWLEDGEMENTS

I would like to express my heartfelt gratitude to several individuals who have played pivotal roles in my academic journey. First and foremost, I extend my sincere appreciation to my advisor, Dr. Badrul Chowdhury, for his unwavering support and guidance. He consistently dedicated his time and shared his extensive knowledge whenever I sought his assistance. Working under his supervision was a remarkable opportunity.

I would also like to acknowledge Dr. Churlzu Lim for generously offering his time and providing valuable constructive feedback. Furthermore, I extend my gratitude to the remaining members of my committee, Dr. Valentina Cecchi and Dr. Madhav Manjrekar, for their valuable time and insightful comments.

Throughout my graduate studies, I received support from the Graduate Assistant Support Plan tuition award provided by the University of North Carolina at Charlotte Graduate School. I am profoundly thankful for this financial assistance, which greatly facilitated my academic pursuits.

I must also express my appreciation for the research assistantship granted within Dr. Badrul Chowdhury's research group and the teaching assistantship offered by the Department of Electrical and Computer Engineering. These opportunities not only enriched my educational experience but also contributed significantly to my growth as a scholar.

TABLE OF CONTENTS

LIST OF TABLES

LIST OF FIGURES

LIST OF ABBREVIATIONS

$'$	Index for commitment states obtained from master problem
b	Index for BES systems
i	Index for MG systems
j	Index for DG systems
k	Index for PV systems
l	Index for battery cycles
s	Index for scenarios
t	Index for time
B	Battery cell replacement cost in $\$/kWh$
C^{DG}	Fuel cost of the DG in $\$/kWh$
C^{G}	Cost of purchasing power from or selling power to the main grid
E	Total energy required for the NEL
k_1, k_2	Battery specific constants
$P^{ch,max}$	Maximum charging power to the BES
$P^{dch,max}$	Maximum discharge power from the BES
$P^{DG,min}$	Maximum power output from a DG
$P^{DG,min}$	Minimum power output from a DG
$P^{G,max,pur}$	Maximum power purchased from the grid
P^{LD}	Essential Load

P^{Loss}	System loss in kW
$P^{NEL,min}$	Minimum NEL in kW
P^{PV}	Power generated from the PV panel
RD	Maximum allowable ramp down rate of the DG
RU	Maximum allowable ramp up rate of the DG
Sc	Total number of scenarios in a case
SE^{max}	Maximum energy capacity of the BES in kWh
$P^{G,max,sell}$	Maximum power sold to the grid
α	Associated dual variable for DG commitment state
β^{ch}	Associated dual variable for BES charging commitment state
β^{dch}	Associated dual variable for BES discharge commitment state
ΔL	Total life loss of the battery
γ	Associated dual variable for NEL commitment state
Φ	Battery depth of discharge stress function
f	Battery degradation cost
I^{ch}	Charge commitment state of the BES
I^{dch}	Discharge commitment state of the BES
I^{DG}	Commitment state of the DG
I^{NEL}	Commitment state of the NEL
m	Mismatch between power generation and load

P^{BES}	Charging power to or discharging power from the BES
P^{DG}	Power generated by the DG
P^{G}	Power purchased from or sold to the main grid
P^{NEL}	Power supplied to the NEL
SE	Energy stored in the BES
VG	Virtual generation slack variable
VL	Virtual load slack variable

CHAPTER 1: Introduction

An electrical grid that's dependable, with ample power generation capacity to meet the everyday load, and capable of enduring unexpected disruptions, represents a fundamentally sound framework for a smart grid in the 21^{st} century. However, this concept, while conceptually robust, remains incomplete. The modern grid should be more than just robust; it should possess the ability to adapt seamlessly to a wide spectrum of challenges, ranging from large-scale environmental incidents to unforeseen, unnatural events, all while remaining operational in the face of adversity.

Furthermore, the smart grid should go beyond mere functionality and aim to minimize the repercussions of catastrophic events that could impact the quality of life, economic activities, national security, and the smooth operation of critical infrastructure. In essence, the grid should not only prioritize reliability in providing a continuous power supply for everyday life but also emphasize resilience. Reliability assures uninterrupted power supply under normal circumstances, fostering stability in daily activities. In contrast, resilience introduces a more encompassing set of ideals, including the capacity to withstand and rebound from extreme or prolonged events. Thus, it's crucial to understand that while all resilient grids are inherently reliable, not all grids characterized by reliability can claim the same degree of resilience. The distinction between the two emphasizes the evolving demands and expectations placed on modern energy infrastructure, ultimately shaping the grid of the future.

1.1 Networked Microgrids

In today's modern distribution systems, there is a growing presence of multiple microgrids (MGs) equipped with extensively integrated inverter-based resources. These

versatile MGs are engineered to operate either independently or in coordination with the main grid, emphasizing the critical role of MG resiliency in ensuring an uninterrupted power supply to end consumers. Additionally, when independent MGs are geographically close, they have the capacity to function collectively as a network, akin to an archipelago when viewed from the perspective of the main grid [1]. The primary goal underpinning the formation of MG networks is to establish an intelligent structure that facilitates the efficient sharing of locally generated power. This collaborative approach bolsters the overall system's stability, reliability, and resilience, particularly during events that could disrupt the balance between power generation and consumption.

Traditionally, the operation of MGs falls within the purview of the Distribution System Operator (DSO), who oversees MG interconnections and orchestrates optimal power exchanges by aggregating crucial data from individual MGs [2]. This centralized control scheme relies on a robust cyber network to facilitate seamless communication and control. Nevertheless, in certain scenarios, decentralized control strategies have been embraced as well [3, 4].

Within the context of a smart community, where resiliency is of paramount importance, one or more MGs can participate in coordinated operations [5, 6]. While connected to the main grid, these operations are geared towards reducing overall energy consumption, curbing emissions, and maximizing the utilization of renewable energy resources [7–9]. Grid-connected MG operations offer the flexibility to adapt and reconfigure as needed to optimize energy consumption and minimize emissions [10]. However, in the face of severe disruptions, a smart city may find itself isolated from the main power grid [11–13]. In such challenging circumstances, the city's energy needs can only be met by the local distributed energy resources (DERs), supporting a reduced set of critical end-use loads. In these scenarios, the smart city is more likely to be served by individual MGs rather than a single uniform MG [14].

Forming a network of MGs offers several compelling advantages, including the integration of diverse DERs into the system [14]. These benefits can be succinctly summarized as follows:

1) Lowering emissions by sharing renewable energy resources.

2) Efficiently utilizing distributed generator (DG) units while adhering to their operational constraints.

3) Providing mutual support to neighboring MGs in the event of a local DG failure.

4) Reducing operational costs through the incorporation of a diverse array of energy choices.

1.2 Resiliency

In a scenario where the main grid serves as an infinite bus with a seemingly boundless power supply and demand capacity, it effectively acts as a balancing force that mitigates power mismatches within individual MGs. Consequently, the loss of the main grid can pose significant challenges for MGs. Existing research on grid resiliency has primarily centered on the structural and configurational aspects of the system [15,16]. What adds an extra layer of complexity to the analysis of resiliency is the presence of physical constraints, encompassing voltage and line limitations, generation and thermal restrictions, within a power distribution system. Furthermore, the control decisions made by the Distribution System Operator (DSO), including network reconfiguration, play a crucial role in influencing the overall resiliency of the system [17].

Despite numerous research studies focusing on the resiliency of complex power system networks [18–21], the effectiveness of different control actions remains challenging to assess and compare using the existing resilience matrix. Various optimization-based network reconfiguration methods have been explored [22, 23], although research incorporating multiple MGs into these strategies is relatively limited. While these approaches can facilitate successful power restoration, some of them may prove vul-

nerable to extreme events [17].

1.3 Rationale

While there has been a substantial body of research on MG cluster optimization, a significant portion of these studies has predominantly focused on cost minimization as their primary objective [24–31]. However, a select few have taken different angles in their approach, with authors in [27,29,32] emphasizing the importance of maximizing reliability. Authors in [30, 31, 33] extended their optimization goals to encompass system adequacy maximization. Previous research efforts like those in [19, 34] have applied techniques such as Bender's Decomposition and robust optimization for single MG optimization.

However, a newer and evolving challenge in the realm of MG optimization is the creation of an optimal framework geared towards ensuring resiliency, particularly for interconnected MGs. Notably, research works such as [35] have addressed optimal battery energy storage (BES) scheduling, while [36] focused on optimal load shedding for multiple MGs. Another significant contribution can be found in [37], where a Model Predictive Control (MPC) method was introduced for the optimal scheduling of distributed generators (DGs) and BES systems in a MG cluster.

Considering the proximity and interconnection of multiple MGs, it becomes evident that a robust, resilient infrastructure is imperative for their sustained operation, especially during events characterized by extreme uncertainty, such as natural disasters. In these scenarios, the possibility of the main grid remaining disconnected for extended periods poses a unique set of challenges. While there are some studies that delve into resilient MG operation with the application of decomposition techniques, only a few have ventured into the domain of large MG networks.

This research stands out as innovative for harnessing the advantages of the Bender's Decomposition technique to achieve cost-effective resiliency in a network of MGs. The utilization of Benders Decomposition notably alleviates the computational complexity

that often plagues larger networks, which typically involve a multitude of variables. As a result, this approach is capable of ensuring zero generation-load mismatches for a wide range of scenarios during extreme events. Additionally, a distinct contribution lies in incorporating battery degradation costs into the cost comparison among various MG layouts, a facet often absent in existing literature.

In this study, we introduce an interconnected MG operational framework using Bender's Decomposition with a key focus on minimizing load curtailment. The contributions of this work can be summarized as follows:

1. The proposal of an innovative method for scheduling multiple MG resources to facilitate resilient operation during extreme events, tested on the modified IEEE 123-bus distribution test system.

2. The achievement of resilient operation, guaranteeing zero generation-load mismatch in numerous potential scenarios resulting from extreme weather events.

3. The comparison of day-ahead scheduling and resilient operation costs for different networked MG layouts across various extreme weather events.

The proposed approach can serve as a valuable tool for MG owners in determining the optimal day-ahead scheduling of MG units. Furthermore, establishing connections with neighboring MGs offers additional benefits from both resiliency and economic perspectives.

The subsequent sections of this dissertation are structured as follows: Chapter 2 provides a comprehensive review of relevant literature. Chapter 3 outlines the proposed methodology and the test system used. Results, cost analyses, sensitivity to uncertainties, and comparison with the Single Stage MILP approach are detailed in Chapter 4, and the concluding remarks are presented in Chapter 5.

CHAPTER 2: Background

2.1 MG Components and Control

A MG is a small network situated at the low voltage side of a distribution substation through a point of common coupling (PCC). MGs contain of a number of components including DGs, energy storage system (ESS), and essential, non-essential loads. The distinguishing features and dynamics of all the components make the control and operation of the MGs difficult. Because MGs incorporate a lot of DERs and ESS, the energy management method can drastically differ from the traditional power system.

2.1.1 Distributed Generators (DGs)

The inclusion of the DGs makes electrical power available in the remote areas, promotes local decision making, and to some extent, protects the environment. As a result, it is becoming a more popular choice for the large-scale grid electrification [38].

Generally, a DG is a small scale (kW) electric power generator connected near the demand side of the distribution network. The power generation capacity of the DGs can vary between 1 kW and 3 MW [39, 40]. Unlike centralized power systems, DGs are smaller in size and flexible in terms of location. This allows the users to generate the required amount of power for their household or community. Thus, cost is lowered by minimizing surplus generation and line losses. A number of studies [41–43] have concluded that even for a user 3.4 miles away from the main grid, decentralized electrification can be more economically beneficial.

The DGs can be powered by different types of fuels such as diesel, natural gas (NG), hydrogen (H_2), solar, wind, geothermal, biomass or a combination of these sources. The DGs fueled by renewable energy (e.g., wind turbines, photovoltaic [PV] panels)

are non-dispatchable, and their output varies with nature. On the other hand, the dispatch level of the fuel based DGs (e.g., micro-gas turbines, diesel generators, etc.) can be determined by the user according to their operating cost. Different types of DGs, their sizes, efficiency and costs are presented in Table 2.1 [44].

Table 2.1: Various types of DGs

Technology	Size range	Energy source	Electrical efficiency	Waste heat quality	Equipment cost ($)
Reciprocating engine	1-5,000+ kW	Diesel, propane, NG, or gasoline	25-45	High	500-1000
Microturbine	30-1000 kW	NG		High	500-1000
Fuel Cell	1W -2 MW	Biogas, diesel,H_2, methanol, NG, and propane	1-60	Depends on technology	1000-5000
Stirling Engine	$\geq$ 100 watts	Diesel, biofuels	10-30	Medium	1200-7000
Photovoltaics	$\geq$ 1 kW	Solar	10-20	N/A	1850-2130

Moreover, some DGs such as combined heat and power (CHP) plants can simultaneously generate electric power and usable heat. This characteristic proves really beneficial, especially because DGs are placed locally. This added benefit of the CHP plants is one of the main economic privileges of installing MGs [45].

An effective energy management system (EMS) is crucial to operate the MG at the optimal energy scheduling. Balancing generation and load while minimizing the operational cost adds challenge to the MG's control algorithm. Advancement in the inverter control strategy has made it possible to successfully integrate variable fre-

quency DERs in the MG. On another note, observing and controlling all the DG units requires proper communication among them. The communications standard for DERs (61850-7-420) established by the International Electro technical Commission (IEC) is commonly followed (Cleveland, 2008) in this regard [46]. It is an international code that determines the communication and control protocols for all the DERs, especially when DERs are connected to the main grid [46].

2.1.2 Energy Storage Systems (ESS)

The energy storage system (ESS) is one of the crucial components in the MG. The benefits of ESS include [47]:

1. Ensuring stable power supply to the load in the face of uncertainty posed by the renewable energy sources.
2. Storing surplus energy during off peak and serving loads during peak hours.
3. Enhancing reliability
4. Serving as a local power source in remote areas or islanded MG
5. Improving power quality by providing fast response
6. Providing voltage and ride through support

A comparison among different ESS technologies is presented in Figure 2.1 [48]. While pumped hydro can store a significant amount of energy, super capacitors are small but can respond very fast.

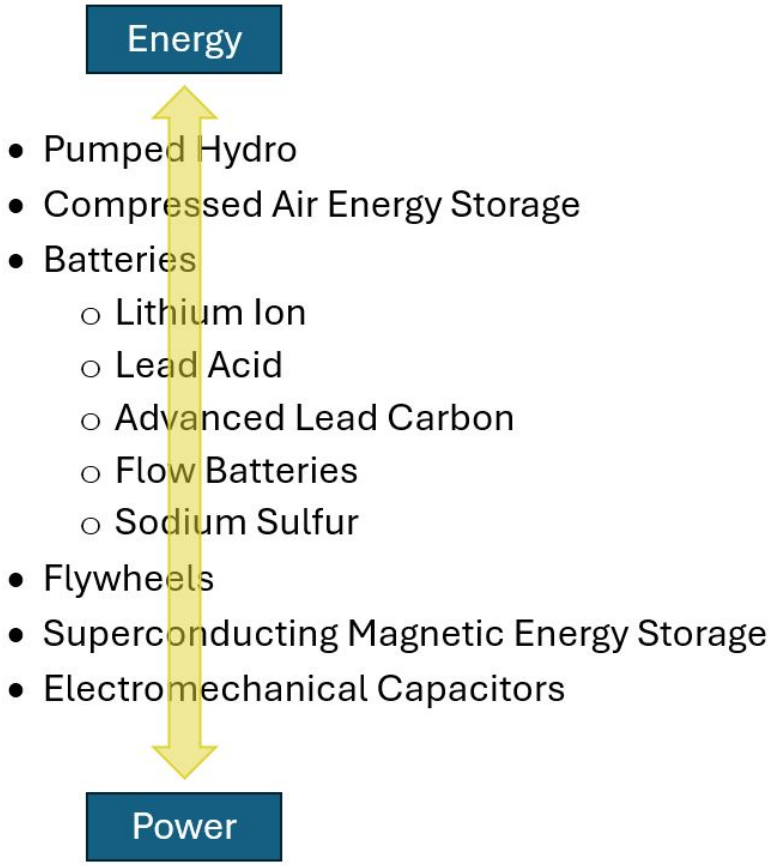

Figure 2.1: Essential load and PV profile

The most common types of ESS used in MGs are battery energy storage (BES) types. Among all the available options, the Li-Ion battery has better characteristics compared to other technologies of batteries [49]. Because of their prolonged cycle life, acceptable cell voltage, heat dissipation capability, excellent charge accumulation, and decent depth of charge, they are more widely used than any other type of energy storage systems [50].

2.1.3 Loads

Generally, a MG includes both critical or essential load and controllable or non-essential load. When the MG is grid connected, there is usually enough generation to meet wll the loads. However, during islanded hours there may not be enough generation to supply all the loads. even after utilizing the DGs and ESS, if there is

insuffcient power, some non-essential loads can be curtailed at the expense of customer's inconvenience.

2.2 Networked MGs Structure

A number of MGs can form a network as depicted in Figure 2.2 [51]. Figure 2.2(a) portrays the parallel-connected MG (PCM) structure. In this architecture, each MG has a single point of common coupling (PCC), and all the MGs are connected to the same power grid in parallel. While grid-connected, these MGs receive orders from a controller in the external grid. A number of authors have used the PCM layout in their papers [52–56]. In Figure 2.2(b), the grid series interconnected MGs

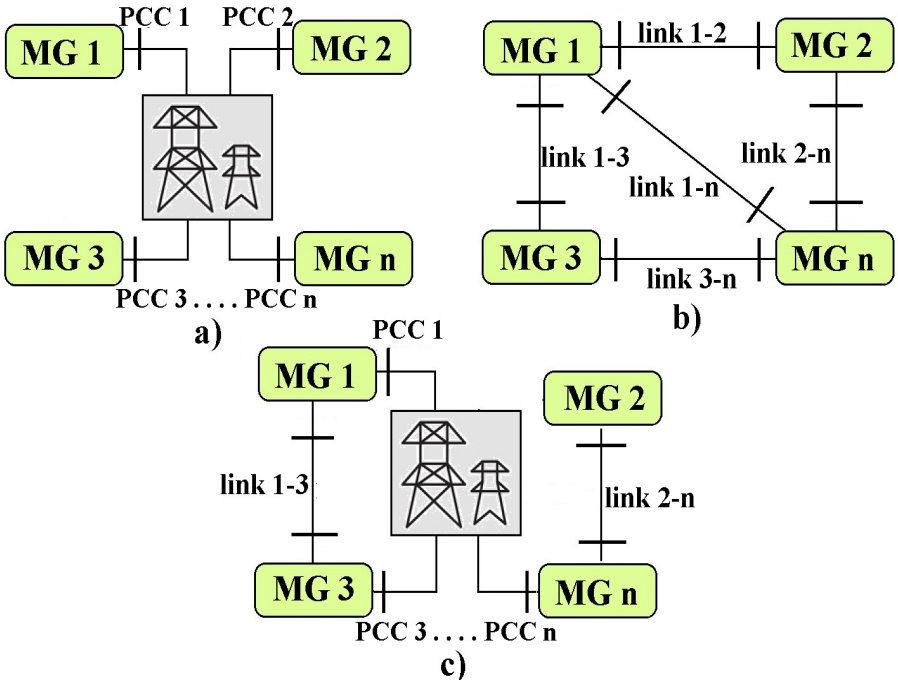

Figure 2.2: Different layouts of MG cluster [51]

(GSIM) architecture is presented. In this case, each MG is connected to another in a point-to-point manner. Because there is no connection with the utility grid in this layout, if the interconnected MGs are AC, they must generate the voltage and the frequency themselves. Such architectures have been studied in [57, 58]. The next possible architecture is shown in Figure 2.2(c) and is termed a mixed parallel-series

connection (MPSC). In this structure, some MGs can form clusters of MGs connected in series. However, each of the single MGs or clusters has at least one direct connection with the grid. The authors in [59] presented an MPSC layout, where a cluster of two MGs is connected to an external power grid.

Ensuring optimal mutual power support among all the MGs in a network introduces an added challenge compared to optimal control in a single MG [60].

2.3 Control and Optimization of Networked MGs

The traditional PID controller used in MGs does not provide optimal results, as the acceptable error is defined at the time of modeling. On the other hand, in the optimal control methods, the control problem is formulated as an optimization problem. The control and management of a MG cover different technical areas, time scales, and physical layers. The local power, voltage, and current of a MG are handled by the primary control which performs control actions by following the set-points determined by upper level controllers. Based on the implementation of these control levels, a MG can be controlled in centralized, decentralized, distributed, or hierarchical fashion. The same idea can be expanded to multi-MG scenarios as depicted in Figure 2.3.

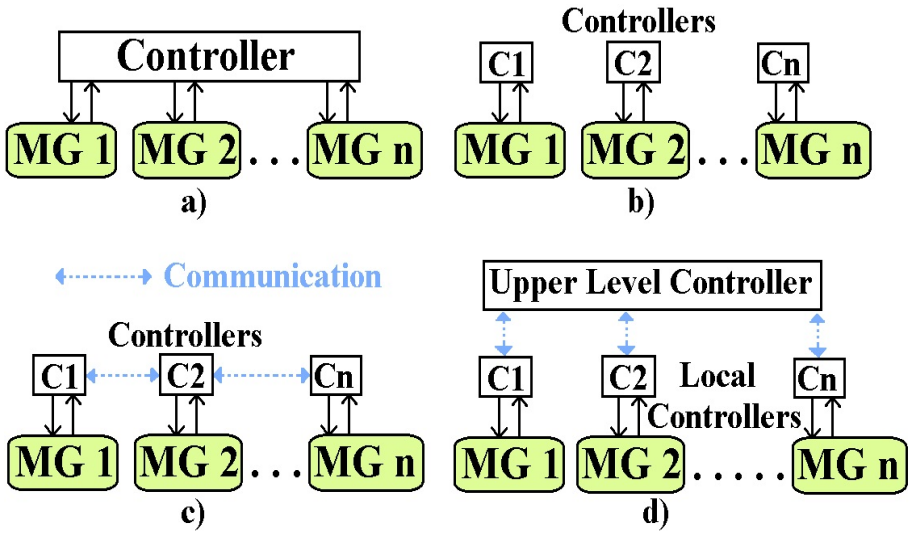

Figure 2.3: Basic MG control structures. (a) Centralized. (b) Decentralized. (c) Distributed. (d) Hierarchical [61].

2.3.1 Centralized Control

In a centralized structure, a central control unit gathers and transmits information from and to all the MGs. The collected information is used to execute the control and management procedures. The centralized control can be implemented in an effortless manner while securing the observability and controllability of the whole system. However, the main disadvantage of centralized control structure is it imposes a single point of failure threat. As a result of the central controller breakdown, all the functionalities are lost. In addition, the centralized control structure is less flexible and demands significant computational resources. Consequently, centralized control is more suitable where the communication is limited and the computational cost is low, such as smaller MG networks. The centralized control structure of a MG cluster is shown in Figure 2.3(a).

Authors in [62–68] researched optimization techniques that use centralized control strategies. An energy management method for a multi-MG system is proposed in [62], which focuses on cost minimization and economic optimization. Again, a dynamic multi-criteria-based energy management approach is proposed in [63] which takes the security, reliability, power loss, energy cost, and environmental concerns into account while decision making. Particle swarm optimization and heuristic-based optimization approaches are adopted in [64,65] in determining the most suitable MG in the neighborhood to support each other during emergencies. A control scheme proposed in [68], is claimed to be able to coordinate multiple MGs by optimizing their renewable energy usage. Nonetheless, all these control techniques are communication-dependent and therefore, the system reliability is compromised.

2.3.2 Decentralized Control

The decentralized control scheme shown in Figure 2.3(b), does not require information from other MGs in the network. The respective MG controller operates with

the information that is locally available. One benefit of the decentralized method is that it does not demand real-time communication. However, as a drawback of lacking coordination between local regulators, global optimization is not achieved.

2.3.3 Distributed Control

In a distributed control scheme, the information flows between the controllers through communication lines. As a result, a coordinated behavior is observed among all the MGs. The main challenge placed by the distributed control scheme is the coordination among MGs to meet either the control or optimization objectives, which demand flawless communication and exchange of essential information. A distributed energy coordination management method based on droop control is proposed in [66, 67, 69, 70]. The drawback in this control is the continuous enforcement of power exchange between two MGs resulting in additional power loss. An updated control strategy has been proposed in [71–73] to address this issue. In this strategy, the power flow between two MGs takes place within a certain operation threshold only.

2.3.4 Hierarchical Control of Networked MGs

The increasing number of inverter-based resources is making the existing power system network more complex and in need of complicated decision-making. It is becoming increasingly evident that all the requirements may not possibly be met in a distributed or decentralized manner. A hierarchical control structure, as shown in Figure 2.3(d), has thus come into the picture. Simple functions can be implemented in the local controllers of the system to ensure basic operations, while the advanced control and management functions can be applied in the central controller. Hierarchical control is thus becoming a standardized configuration in MGs.

2.4 MG Reliability and Resilience

In recent times, the intensity and frequency of natural disasters have been increasing, posing a significant threat to the energy infrastructure [74]. Especially the electric

power system is generally prone to outages and resulting losses. Natural disasters, ranging from extreme temperatures and storms to cyclones, earthquakes, volcanic eruptions, floods, droughts, tsunamis, and even biological crises such as epidemics and pandemics [75], consistently inflict significant damage on the electric power sector year after year. The impact of these disasters on the power infrastructure is profound. In Table 2.2, a historical account of the most widespread blackouts in the United States can be observed, some of which led to extended power outages [76].

Table 2.2: Largest blackouts in the history of U.S.A. [74]

Blackout/Cause of blackout	Lost electricity service(million customer hours)
Hurricane Maria (2017)	3,393
Hurricane Georges (1998)	1,050
Hurricane Sandy (2012)	775
Hurricane Irma (2017)	753
Hurricane Hugo (1989)	700
Hurricane Ike (2008)	683
Hurricane Katrina (2005)	681
Northeast blackout (2003)	592
Hurricane Wilma (2005)	515
Hurricane Irene (2011)	483

Notably, what stands out is that hurricanes were responsible for nine out of the top ten blackouts. This is particularly worrisome given that eight of the ten most disastrous hurricanes ever recorded have occurred within the last 10 years [77]. Aside from the peril posed by natural disasters, the power system is also susceptible to other malevolent threats that can trigger power outages and blackouts. These threats encompass both physical and cyber-attacks, adding another layer of complexity and

vulnerability to the power grid.

Historically, power system reliability has been ensured using single or double outage contingency (N-1 or N-2). The power system is termed N-1 or N-2 secured if it can endure a single or double component failure. Even though the probability of such incidences is high, the impact is much lower. Therefore, the grid remains unharmed and a small number of customers may lose power for a short period of time. However, it becomes essential to conduct multiple outage contingencies (N-K) for catastrophic events such as the natural disasters mentioned above. During such events, the priority is to keep the critical infrastructures functional and operational. Additionally, ensuring minimum losses and avoiding a disastrous aftermath following the event are important factors to be considered [78]. Therefore, it is crucial to identify the underlying differences between reliability and resilience. Due to the increasing phenomena of natural disasters and resulting outages, a thorough study of power system resilience has become essential.

On another note, the advancement of smart grid technologies and its applications advocate for a resilient power system. Since a MG is an indispensable part of the smart grid, it can play a major role in this regard. In fact, numerous recent studies suggest the appropriate utilization of MGs and DERs can play a vital role in improving system resiliency [74].

2.5 MG Day-ahead Scheduling

Optimal scheduling and energy management strategies of MGs demands various operational difficulties to be overcome. Generally, a unit commitment problem is solved for the grid connected operation of the MG to determine the required local generation at the minimum cost. However, to ensure resilient operation, MG day ahead scheduling should also take into account the islanded hours of operation. The scheduling should be such that the maximum number of loads are supplied during the islanded hours.

2.5.1 Feasible Islanding of the MG

Ensuring feasible islanding of a MG during any severe event is the first step towards achieving complete resiliency of the MG. Aside from the technical constraints, the feasible islanding mostly depends on confirming adequate local supply to the critical loads of the MG in the absence of the main grid. Any mismatch between the generation and the load may result in frequency fluctuations, leading to significant failure of multiple system components [74]. To prevent such occurrence during extreme events, the MG must be scheduled accordingly while it is still in the normal operation mode. If the initial unit commitment results from the normal operation does not guarantee feasible islanding, the results are revised accordingly.

2.5.2 Uncertainty

Uncertainty refers to certain aspects of MG management which can neither be projected precisely, nor be controlled. There are mainly two types of uncertainties [79,80]:

1. Uncertainties that originate from forecast errors, such as load demand, renewable generation, and real-time market price.

2. Uncertainties that result from disruption in the supply or service restoration time

A MG scheduling is proposed in [81] that ensures system resilience and conducts sensitivity analysis for various degrees of uncertainty. Two deep reinforcement learning techniques for resilient MG management are proposed and analyzed by Tightiz and Yang [82] while taking uncertainty into account. On another note, some research projects emphasize timing ESSs in order to address the uncertainty in the generation of RESs. An effective optimization approach to MG scheduling is presented in [83] that takes into account demand projections and renewable power generation uncertainties at the appropriate robustness level.The effect of accurately estimating and

choosing the ESS of the islanded MGs on their uncertainties-based resilience metrics is quantitatively assessed by Shahinzadeh et al. [84]. With an emphasis on ESS scheduling, a chance-constrained optimization model for MG robust and economical operation is presented in [85]. In order to estimate certain optimization issue inputs, such as load demand, PV generation, and supply disruption, this study use machine learning models.

2.5.3 Networked MG Scheduling

Because networked MGs allows each MG in the neighborhood to aid one another through local sources, it offers substantial prospects toward a more resilient power grid. This networking does present certain difficulties, though. Whether the communication, control, and decision-making will be centralized or decentralized is linked with privacy concerns. As a result, this has an impact on how the MGs operate and communicate with each other. Furthermore, networking among the individual MGs and the main grid after an incident should be influenced by the market strategy from a practical perspective [74]. There are certain technological difficulties to resolve.

In order to increase system resilience, networking MGs is becoming a more crucial technique [74]. Numerous published studies have been done to optimize networked MG operation. For networked MGs connected to a point of common coupling, a normal and self-healing operation strategy is suggested in [86]. This study states that when an MG experiences a malfunction or generation shortfall, it switches to a self-healing state and asks nearby MGs that are normally running for power support. Through a two-stage decentralized control and networking method, the requested power is optimally distributed across the supporting MGs. A 3-layer optimal scheduling model for networked MGs as a stochastic MILP issue is presented in [87]. In order to provide a small number of the most anticipated scenarios for each stage transition, this study used the three-point estimation strategy to feed the suggested model. For the best possible operation of networked MGs in both normal and critical situations,

a dynamic, stochastic MILP is advised in [88] that captures uncertainties of the start time and length of large disturbances. Authors in [89] present an networked MG scaling model in a design based research project with the goal of improving system resilience. In [90], authors explore the effects of the Internet of Things (IoT) on networked MG operation. Taking the demand response program into consideration, a day-ahead scheduling is recommended in [91] as a solution to the prolonged detachment of networked MGs from the main grid. In [92], a two-stage operational strategy is proposed using Bender's Decomposition to test the viability of MG islanding.

2.6 Multi-objective Optimization Problems

All the design problems that exist around us are multi-objective by nature. In system engineering, the four main objectives are performance, cost, schedule and risk. As shown in Figure 2.4, an inherent tension exists among these four main objectives [93]. If the schedule and the risk level are fixed, the cost increases to

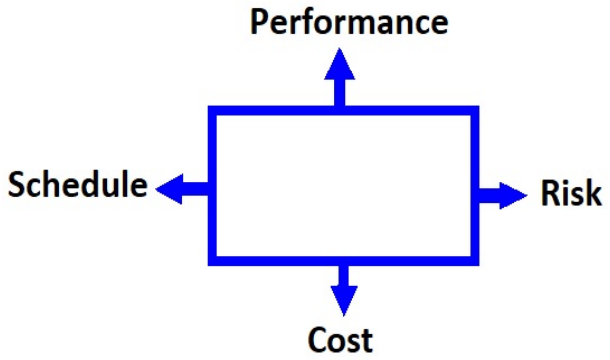

Figure 2.4: Tensions during system design [93]

achieve better performance. Extending one of the four sides in the rectangle of Figure 2.4 would compromise the other sides. Performance of a product can be measured differently. Obtaining a balance among these performances, risk and cost is a part of the engineering department. When scheduling is involved, it becomes a job of the project management. However, assessing, observing and finding solutions of these trade-offs is one of the main responsibilities of system designers. This multi-objective

thought process is very significant, as it ensures optimal designs.

A common multi-objective optimization problem may be formulated as in:

$$\begin{aligned} \min\ & \mathbf{C}(\mathbf{x}, \mathbf{p}) && \text{Where,} \\ \text{s.t. } & \mathbf{f}(\mathbf{x}, \mathbf{p}) \leq 0 && \mathbf{C} = [C_1(\mathbf{x})...C_k(\mathbf{x})]^T \\ & \mathbf{f}'(\mathbf{x}, \mathbf{p}) = 0 && \mathbf{x} = [x_1...x_i...x_m]^T \\ & x_{i,L} \leq x_i \leq x_{i,U}\ (i = 1, ..., m) && \mathbf{f} = [f_1(\mathbf{x})...f_{n_1}(\mathbf{x})]^T \\ & \mathbf{x} \in S && \mathbf{f}' = [f'_1(\mathbf{x})...f_{n_2}(\mathbf{x})]^T \end{aligned} \tag{2.1}$$

Here, the multi-objective function $\mathbf{C}_i \in \mathbb{R}$ is a column vector. It has k objectives. Each of these objectives is dependent on a vector $\mathbf{x}$ of m decision variables and a vector of constant parameters, $\mathbf{p}$. The decision variables are presumed continuous and can be adjusted freely by the user within upper and lower limits, x_U and x_L, respectively. The two vectors f and f' are set of n_1 inequality and n_2 equality constraints respectively which need to be satisfied for $\mathbf{x}$ to be in the feasible domain S. The problem is to minimize all components of the objective vector at the same time. This is the reason it is called multi-objective optimization problem. It is also popularly known as multi-criteria optimization, vector minimization, multi-attribute maximization etc.

2.6.1 Goal Programming

Goal programming is an addition of linear programming which deals with multi-objective optimization with contrasting objectives. Each of these individual objectives is assigned a goal or set value to be achieved. Any unwanted deviations from these set values are then minimized using an achievement function. Depending on the user's requirement or the type of goal programming, this function can be a vector or a weighted sum.

The type of goal programming model is picked by the user based on their goals. In

the basic goal programming formulations, the undesirable deviations are arranged by their level of criticality. This means minimizing the deviations of factors which are more important to the user are prioritized over the other factors. This is termed as lexicographic (preemptive) or non-Archimedean goal programming [94].

A general mathermatical formulation of the Goal Programming can be found in [95]: Instead of the original objective function $c_i(\bar{x})$ where decision variable vector $\bar{x} = x_1, ..., x_i, ...x_I$, in Goal Programming an achievement function $\bar{a}$ is minimized:

$$\bar{a} = f_1(\bar{n}, \bar{p},), ...f_j(\bar{n}, \bar{p}), ...f_J(\bar{n}, \bar{p}) \tag{2.2}$$

such that:

$$\begin{aligned} c_k(\bar{x}) + n_k - p_k = b_k \quad \text{for all } k = 1, ..., m \\ \bar{x}, \bar{n}, \bar{p} \geq \bar{0}, \end{aligned} \tag{2.3}$$

Here n_k and p_k are the negative and positive deviation variables associated with constraint k. f_i is a function of the deviation variables associated with the objectives or constraints with i^{th} priority level. The aim is to minimize the deviation variables to obtain the desired goal. The process is summarized in Table 2.3.

Table 2.3: Minimizing deviation variables in Goal Programming [95]

Goal or constraint type	Processed goal or constraint	Deviation variables to be minimized
$c_k(\bar{x}) \leq b_k$	$c_k(\bar{x}) + n_k - p_k = b_k$	p_k
$c_k(\bar{x}) \geq b_k$	$c_k(\bar{x}) + n_k - p_k = b_k$	n_k
$c_k(\bar{x}) = b_k$	$c_k(\bar{x}) + n_k - p_k = b_k$	$p_k + n_k$

2.7 McCorkmick Envelope Relaxation of Bilinear Problems

Bilinear problems are non linear problems (NLP) and non-convex by nature. This makes the solution difficult and some type of convex relaxation technique may be

applied. The McCormick Envelope, proposed first by Dr. Garth McCormick, is such a method. In this method, it is assumed that convex and concave envelopes can be drawn for the given function [96]. The concave and convex envelope, are the concave over-estimator and convex under-estimator respectively which provides the closest fit to the given function. Like an envelope enclosing a letter, the envelope encircles the provided function and constrains the possible solution space to the greatest extent. For a given function and domain, there can be several concave over-estimators and several convex under-estimators, but only one concave envelope and one convex envelope. The link between the given function f(x), a convex envelope, a concave envelope, multiple concave over-estimators, and multiple convex under-estimators is shown in Figure 2.5. Four sets of constraints are introduced, and a new variable is substituted

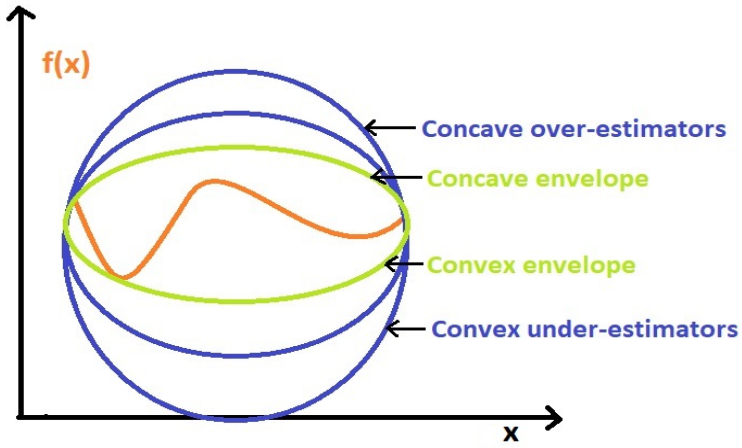

Figure 2.5: McCormick Envelope Method design [97]

for each bilinear term. Thus, the bilinear NLP problem is relaxed into a convex LP problem which can be more convenient to solve. Below is an example of a non-convex function:

$$min \quad C = \sum_{i=1} \sum_{j=1} p_{i,j} x_i y_j + f_0(z) \tag{2.4}$$

subject to,

$$\sum_{i=1} \sum_{j=1} p^l_{i,j} x_i y_j + f_l(z) \leq 0 \quad \forall l \in L \tag{2.5}$$

$$x^L \leq x \leq x^U$$

To apply McCormick Envelope method to the aforementioned non-convex problem, $x_i y_j$ is substituted by w_{ij}. As a result the convex problem below is achieved:

$$min \quad C = \sum_{i=1} \sum_{j=1} p_{i,j} w_{i,j} + f_0(z) \tag{2.6}$$

subject to,

$$\begin{aligned} \sum_{i=1} \sum_{j=1} p^l_{i,j} w_{i,j} + f_l(z) \leq 0, \quad \forall l \in L \\ w_{i,j} \geq x^L_i y_j + x_i y^L_j - x^L_i y^L_j \\ w_{i,j} \geq x^U_i y_j + x_i y^U_j - x^U_i y^U_j \\ w_{i,j} \leq x^L_i y_j + x_i y^U_j - x^L_i y^U_j \\ w_{i,j} \leq x^U_i y_j + x_i y^L_j - x^U_i y^L_j \end{aligned} \tag{2.7}$$

After the relaxation, the resulting problem is a convex optimization problem.

2.8 Mixed Integer Linear Programming

Linear programming (LP) deals with the problem of maximizing or minimizing a linear function over a polyhedron. For instance:

$$\max \{cx | Ax \leq b\}, \min \{cx | x \geq o; Ax \leq b\}$$

Here, A is a matrix, b, c are vectors and x, y are the variables. In Fourier [1826b, 1827], there are indications of the concept of linear programming. However, it wasn't until the 1940s that Dantzig, Kantorovich, Koopmans, and von Neumann's work helped establish the discipline and acknowledge its significance. As a consequence of the Fundamental theorem of linear inequalities [76], the Duality theorem of linear programming was then proposed and demonstrated by Gale, Kuhn, and Tucker [1951] [98]:

$$\max\{cx | Ax \leq b\} = \min \{yb | y \geq 0, yA = c\}$$

The variables (x and y) in the LP problem can be continuous or discrete. A mixed

integer linear programming (MILP) problem is an optimization problem containing both integer and continuous decision variables, a linear objective function, and linear constraints. MILP theory and practice have evolved throughout the course of its more than 50 years of existence, making it an essential tool in both engineering and business today [99–101]. The modeling flexibility of MIP and LP-based solvers are two factors contributing to the success of MILP. Presently, we possess numerous highly efficient cutting-edge solvers [102–104] that integrate numerous sophisticated methods [105–111]. In fact, MILP has been employed to simulate an extensive array of applications since its inception [112, 113]. While creating appropriate MILP formulations is often not too difficult, caution must be given in this process since some formulation features can drastically lower the efficiency of LP-based solvers. Fortunately, by following basic criteria found in mainstream textbooks, one can usually create formulations that perform nicely with available solvers. However, more sophisticated methods are occasionally required and can frequently perform more effectively than textbook approaches [114].

2.8.1 Single Stage MILP

Regular MILP problems can be solved in a single stage and has the form as follows:

$$\min \sum_{i=1}^{n} c_i x_i + \sum_{j=1}^{m} d_j y_j \tag{2.8}$$

$$\begin{aligned} \text{Subject to,} \quad & \sum_{i=1}^{n} a_{li} x_i + \sum_{j=1}^{m} e_{lj} y_j = b_l \qquad && l = 1, ..., q \\ & x_i^{down} \leq x_i \leq x_i^{up}, \quad x_i \in \mathbb{N}; && i = 1, ..., n \\ & y_j^{down} \leq y_j \leq y_j^{up}, \quad y_j \in \mathbb{R}; && j = 1, ..., m \end{aligned} \tag{2.9}$$

Here, $\mathbb{N}$ is the set of natural numbers (Integers starting from zero to infinity), and $\mathbb{R}$ is the set of real numbers (Both integers, fractions and irrational numbers). However, both the integer and continuous variables are bounded by the limiting constraints,

reflecting most engineering problems. On another note, any integer variable can be represented as a multiplication factor of binary variables 1. For instance, $x = a_1, a_2, ...a_n$ can be substituted by n binary variables:

$$\begin{aligned} x = \sum_{i=1}^{n} a_i u_i \qquad & \text{where,} \sum_{i=1}^{n} u_i = 1 \\ u_i \in 0, 1; \quad & i = 1, ...n. \end{aligned} \tag{2.10}$$

If a centralized solution of problem is not advisable, the integer variables can be considered as complicating variables and the Bender's decomposition scheme can be used used. The details are presented in chapter 2.7.2.4.

2.8.2 Decomposition Techniques

Whether or not an LP or MILP problem is decomposable can be determined from the complicating constraints and complicating variables. If a problem is decomposable, the objective function can be broken down into multiple sections with associated constraints. However, complicating constraints and complicating variables prevent that from happening. In such cases, problem can be decomposed if the complicating constraints or complicating variables are fixed.

2.8.2.1 Complicating Constraints

In real life, linear programming problems can be significantly large in size. It is possible to come across problems that deal with numerous variables and constraints. Using some techniques may make these problems possible or even easier to solve. On another note, a large problem may be more approachable if divided into smaller sections for both theoretical and practical reasons. The techniques which enable certain type of problems to be solved in a decentralized manner, are termed as Decomposition techniques. These techniques may make the solution procedure rigorously simple. These techniques can be implemented only when the problem under study has the suitable structure. There are two such possibilities: the complicating constraint

and the complicating variable structures. The Complicating Constraints structure involves a problem where there is at least one constraint which contains all the variables from the objective function and thereby prevents the separation of the multiple objectives. Because these constraints complicate the solution of the problem, this structure is termed as Complicating Constraints. Below is an example of a problem with complicating constraints structure:

$$\text{minimize} \quad \alpha_1 x_1 + \alpha_2 x_2 + \alpha_3 x_3 + \beta_1 y_1 + \beta_2 y_2 + \gamma_1 v_1 + \gamma_2 v_2 + \gamma_3 v_3 \tag{2.11}$$

$$\begin{aligned} \text{Subject to,} \quad & a_{11}x_1 + a_{12}x_2 + a_{13}x_3 = m_1 \\ & a_{21}x_1 + a_{22}x_2 + a_{23}x_3 = m_2 \\ & b_{11}y_1 + b_{12}y_2 = n_1 \\ & c_{11}v_1 + c_{12}v_2 + c_{13}v_3 = o_1 \\ & c_{21}v_1 + c_{22}v_2 + c_{23}v_3 = o_1 \\ & d_{11}x_1 + d_{12}x_2 + d_{13}x_3 + d_{14}y_1 + d_{15}y_2 + d_{16}v_1 + d_{17}v_2 + d_{18}v_3 = p_1 \\ & x_1, x_2, x_3, y_1, y_2, v_1, v_2, v_3 \geq 0 \end{aligned} \tag{2.12}$$

The last equality constraint has all the variables in it, which prevents from decomposing the problem. Therefore, that is the complicating constraint. Relaxing this constraint can can facilitate decomposing the problem into three subproblems:

Sub-problem 1:

$$\text{minimize} \quad \alpha_1 x_1 + \alpha_2 x_2 + \alpha_3 x_3 \tag{2.13}$$

$$\begin{aligned} \text{Subject to,} \quad & a_{11}x_1 + a_{12}x_2 + a_{13}x_3 = m_1 \\ & a_{21}x_1 + a_{22}x_2 + a_{23}x_3 = m_2 \\ & x_1, x_2, x_3 \geq 0 \end{aligned} \tag{2.14}$$

Sub-problem 2:

$$\text{minimize} \quad \beta_1 y_1 + \beta_2 y_2 \tag{2.15}$$

$$\begin{aligned} \text{Subject to,} \quad & b_{11} y_1 + b_{12} y_2 = n_1 \\ & y_1, y_2 \geq 0 \end{aligned} \tag{2.16}$$

Sub-problem 3:

$$\text{minimize} \quad \gamma_1 v_1 + \gamma_2 v_2 + \gamma_3 v_3 \tag{2.17}$$

$$\begin{aligned} \text{Subject to,} \quad & c_{11} v_1 + c_{12} v_2 + c_{13} v_3 = o_1 \\ & c_{21} v_1 + c_{22} v_2 + c_{23} v_3 = o_1 \\ & v_1, v_2, v_3 \geq 0 \end{aligned} \tag{2.18}$$

Approaches such as Dantzig Wolf or Column Generation methods are taken to solve problems with complicating constraints structure.

2.8.2.2 Complicating Variables

In a linear programming problem, the complicating variables are those variables which hinders the distributed or straightforward solution of the problem. The Complicating Variables structure involves a problem where there is at least one variable from the objective function which is present in all the constraints. Because these variables complicate the solution of the problem, this structure is termed as Complicating Variables.

$$\text{minimize} \quad \alpha_1 x_1 + \alpha_2 x_2 + \beta_1 y_1 + \gamma_1 v_1 + \gamma_2 v_2 + \lambda_1 z_1 \tag{2.19}$$

$$\begin{aligned}
\text{Subject to,} \quad & a_{11}x_1 + a_{12}x_2 + d_{11}z_1 \leq m_1 \\
& a_{21}x_1 + a_{22}x_2 + d_{21}z_1 \leq m_2 \\
& a_{31}x_1 + a_{32}x_2 + d_{31}z_1 \leq m_3 \\
& b_{11}y_1 + d_{41}z_1 \leq n_1 \\
& b_{21}y_1 + d_{51}z_1 \leq n_2 \\
& c_{11}v_1 + c_{12}v_2 + d_{61}z_1 \leq o_1 \\
& c_{21}v_1 + c_{22}v_2 + d_{71}z_1 \leq o_1 \\
& c_{31}v_1 + c_{32}v_2 + d_{81}z_1 \leq o_1
\end{aligned} \tag{2.20}$$

The variavle z_1 is present in all the constraints, preventing a distributed solving approach. Therefore, if it can be given a fixed value z', the problem can be decomposed into 3 sub-problems:

Sub-problem 1:

$$\text{minimize} \quad \alpha_1 x_1 + \alpha_2 x_2 \tag{2.21}$$

$$\begin{aligned}
\text{Subject to,} \quad & a_{11}x_1 + a_{12}x_2 \leq m_1 - d_{11}z' \\
& a_{21}x_1 + a_{22}x_2 \leq m_2 - d_{21}z' \\
& a_{31}x_1 + a_{32}x_2 \leq m_3 - d_{31}z'
\end{aligned} \tag{2.22}$$

Sub-problem 2:

$$\text{minimize} \quad \beta_1 y_1 \tag{2.23}$$

$$\begin{aligned}
\text{Subject to,} \quad & b_{11}y_1 \leq n_1 - d_{41}z' \\
& b_{21}y_1 \leq n_2 - d_{51}z'
\end{aligned} \tag{2.24}$$

Sub-problem 3:

$$\text{minimize} \quad \gamma_1 v_1 + \gamma_2 v_2 \tag{2.25}$$

$$\begin{aligned} \text{Subject to,} \quad & c_{11}v_1 + c_{12}v_2 \leq o_1 - d_{61}z' \\ & c_{21}v_1 + c_{22}v_2 \leq o_1 - d_{71}z' \\ & c_{31}v_1 + c_{32}v_2 \leq o_1 - d_{81}z' \end{aligned} \tag{2.26}$$

To solve problems with complicating variable structure, Bender's Decomposition method may be used. If the problem in concern is a LP problem, the dual of the problem would be another LP problem with complicating constraint structure, and Dantzig Wolf or Column Generation method could be implemented. However, such is not the case with MILP problems [115].

2.8.2.3 Lagrangian Duality

In an unconstrained optimization problem $min\ L(\theta)$ the solution can be determined by solving the first-order optimality conditions. In other words, the solution can be obtained if the gradient is set to zero [116]:

$$\nabla L(\theta) = \frac{d}{d\theta} L(\theta) = 0 \tag{2.27}$$

However, in a constraint problem $minL(\theta)$ subject to $g(\theta) = 0$, the gradient may not be set to zero. Instead it is suffice if the gradient is orthogonal to the constraint. As shown in Figure.2.6, gliding along the constraint at any direction does not change the objective. The constraint g has the orthogonal direction at $\nabla g(\theta)$. This results in the following first-order optimality conditions:

$$\nabla L(\theta) = \lambda \nabla g(\theta) \quad \text{for some } \lambda \in \mathbb{R} \tag{2.28}$$

$$g(\theta) = 0 \tag{2.29}$$

Therefore, both the gradient of the original function and the constraint are parallel to each other. This new variable "λ" is termed as Lagrange multiplier or dual variable.

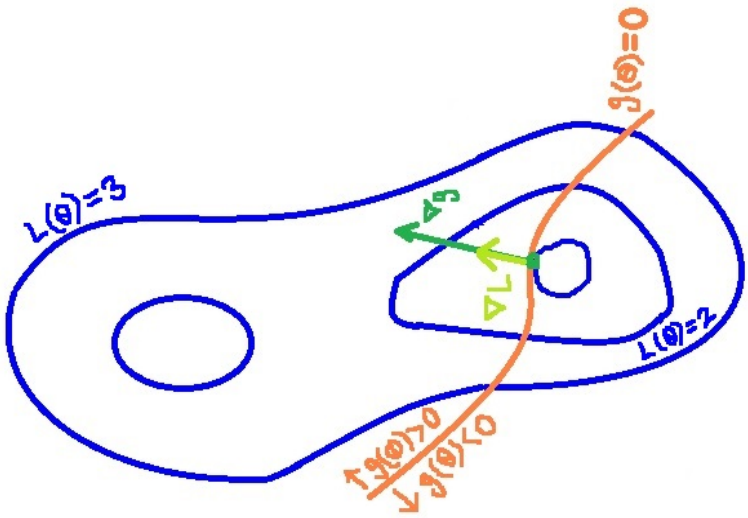

Figure 2.6: Parallel gradients and Lagrange multiplier [116]

A force can be assumed which pushes the point of interest downhill towards the gradient decent. The dual variable will then be a force that pushes back, keeping from violating the constraint. At the optimum, the two forces balance exactly:

$$\lambda \nabla g(\theta) - \nabla L(\theta) = 0 \tag{2.30}$$

By introducing the dual variable, the optimization problem is transformed into a system of simultaneous equations, where the objective and the constraints are treated the same way. This sort of transformation can sometimes make the problem easier to solve [116].

2.8.2.4 Bender's Decomposition

To solve problem 2.8 - 2.9 in a distributed manner, the Benders decomposition method can be implemented following the algorithm below [117]:

1. Integer variables are assigned fixed values.

2. The optimal objective function value is obtained by solving the subsequent continuous LP problem for the fixed integer variables. Because of fixing integer variables, a sensitivity associated with each constraint is also obtained in the form of dual vari-

ables. In addition, an upper bound of the objective function is determined.

3. The MILP master problem is solved to obtain improved values of the integer variables. In addition, a lower bound of the objective function is determined.

4. The optimal solution has been obtained if the bounds of the objective function optimal value are sufficiently close; if not, the algorithm moves on to Step 2.

A formal description of the Benders decomposition algorithm for MILP problems is as follows [117].

Step 1: Initialization

Iteration counter $iter = 1$ is started, with following assumption:

$$x_i^{(v)} = \begin{cases} x_i^{down} & if c_i \geq 0 \\ x_i^{up} & if c_i \leq 0 \end{cases} \tag{2.31}$$

$$\alpha^{(v)} = \alpha^{down} \tag{2.32}$$

$$minimize \quad \sum_{i=1}^{n} c_i x_i + \alpha \tag{2.33}$$

subject to,

$$\begin{aligned} x_i^{down} \leq x_i \leq x_i^{up}, \quad x_i \in \mathbb{N}; \quad i = 1, ..., n \\ \alpha \geq \alpha^{down} \end{aligned} \tag{2.34}$$

Step 2: Sub-problem is solved

$$minimize \quad \sum_{j=1}^{m} d_j y_j \tag{2.35}$$

subject to,

$$\begin{aligned} \sum_{j=1}^{m} e_{lj} y_j = b_l - \sum_{i=1}^{n} a_{li} x_i; \quad l = 1, ...q \\ y_j^{down} \leq y_j \leq y_j^{up}, \quad y_j \in \mathbb{R}; \quad j = 1, ..., m \\ x_i = x_i^{(v)} : \ \lambda_i; \quad i = 1, ..., n. \end{aligned} \tag{2.36}$$

The solution of this problem is $y_1^{(v)}, ..., y_m^{(v)}$ with associated dual variables $\lambda_1^{(v)}, ..., \lambda_n^{(v)}$.

The aforementioned problem can be broken down into smaller parts. If so, the problem can be tackled in parts. If it is not feasible, the user can employ penalties for the objective function and extra variables to make it feasible.

Step 3: Convergence is checked.

Upper and lower bounds of the original objective function is determined.

$$z_{up}^{(v)} = \sum_{i=1}^{n} c_i x_i^{(v)} + \sum_{j=1}^{m} d_j y_j^{(v)} \tag{2.37}$$

$$z_{down}^{(v)} = \sum_{i=1}^{n} c_i x_i^{(v)} + \alpha^{(v)} \tag{2.38}$$

Otherwise, the algorithm continues with the next step.

Step 4: Master problem is solved. The iteration counter is incremented by 1.

$$minimize \quad \sum_{i=1}^{n} c_i x_i + \alpha \tag{2.39}$$

subject to,

$$\begin{gathered} \alpha \geq \sum_{j=1}^{m} d_j y_j^{(k)} + \sum_{i=1}^{n} \lambda_i^{(k)} (x_i - x_i^{(k)}); \quad k = 1, ...v-1 \\ x_i^{down} \leq x_i \leq x_i^{up}, \quad x_i \in \mathbb{N}; \quad i = 1, ..., n \\ \alpha \geq \alpha^{down} \end{gathered} \tag{2.40}$$

The solution to problem is $x_i^{(v)}, ..., x_n^{(v)}$ and α. The algorithm continues with Step 1.

CHAPTER 3: Methodology

A centralized control strategy, as shown in Figure 3.1, is assumed for the interconnected MGs, where all the MGs communicate through a central control unit. This control unit gathers and transmits information from and to all the MGs. The collected information is used to execute the control and management procedures. Some examples of such controllers would be the RTACs (Real-Time Automation Controllers) by SEL (Schweitzer Engineering Laboratories), ECC (Energy Control Center) by Schneider Electric, or the Omnisive Hybrid Control solution by Siemens. In addition, if a single point failure occurs at the central controller, there is provision for a backup central controller which can take over the responsibility. Even though the probability of the backup controller failure is slim, if it does indeed fail, the MGs will operate on their own using their own individual MG controllers. As shown in Figure 3.1, each of the MGs has its own DGs, BES systems, PVs, and non-essential loads (NEL), and is able to share its resources with the neighboring MGs.

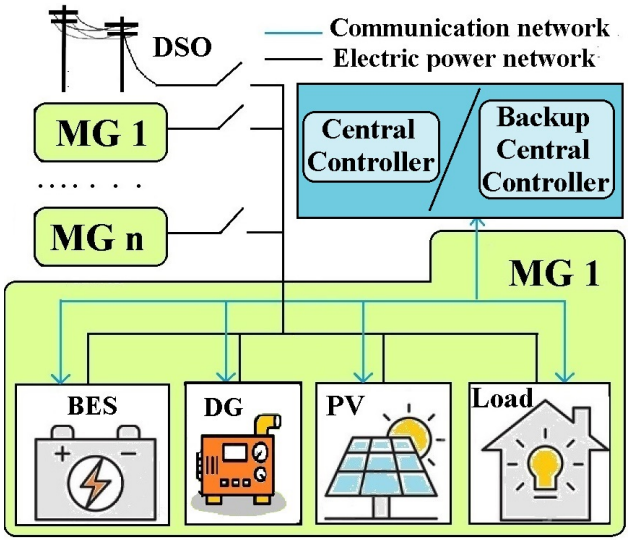

Figure 3.1: Centralized control of the interconnected MGs

3.1 Problem Statement

The resilient operation of this interconnected multi-MG system demands all the MGs to operate in the islanded mode for prolonged hours, preferably without compromising any loads. Since the exact time of any environmental and unnatural event cannot be precisely known in advance, the number of possible islanding scenarios can be many. The more scenarios the optimization problem is solved for, the more resilient the system will be. For each of these scenarios, the total generation should match the total load of the system. This condition is subject to all the power flow and system constraints and losses. If there exists a mismatch between the generation and the load for any scenario, load shedding would need to take place. Nonetheless, the MG owners will benefit not only from resiliency, but also by computing the most cost-effective way to achieve it. The original optimization problem consists of two minimization problems:

1) Minimizing the cost function, J, which includes the cost of MG units and power transfer from the main grid during normal operation

2) Minimizing the generation-load mismatch in resilient operation for each of the possible scenarios considered.

3.1.1 Single Stage MILP Approach

The problem at hand is a multiple-objective, MILP problem which can be solved in various ways. The most straightforward approach is the Single Stage MILP approach, where the problem is solved as a single block. The steps in Single Stage MILP approach to solve the aforementioned problem can be summarized as shown by the block diagram in Figure. 3.2.

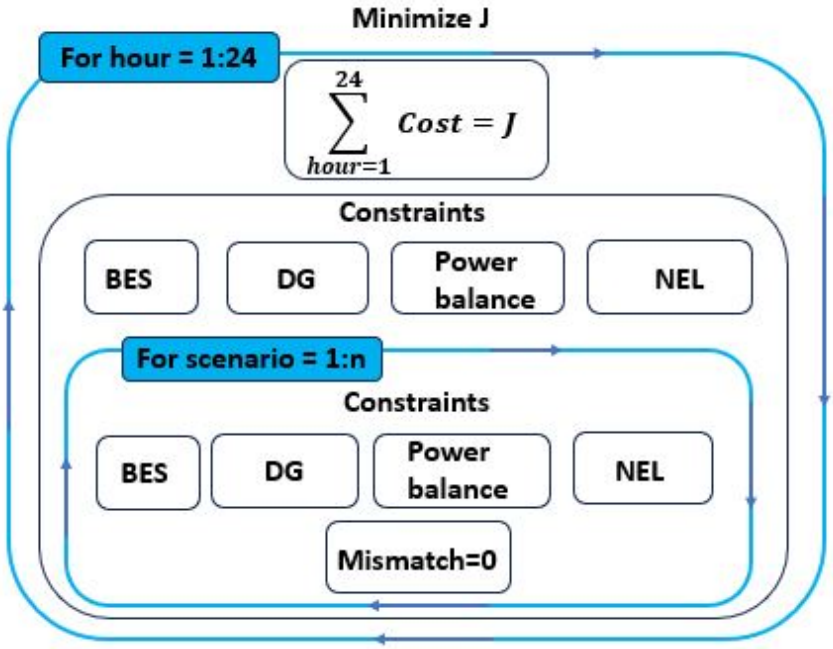

Figure 3.2: Single Stage MILP Approach

In multi-objective problems, one of the main perplexity is representing two different objectives as a whole. In the SMILP approach shown in Figure. 3.2, the mismatch is added as one of the constraints, instead of another objective. This makes the problem more straightforward as it becomes a single objective MILP problem where the only objective is to minimize the cost. In this way the complexity of representing both objectives as a summation can be avoided. However, the drawback to this approach is - if zero mismatch cannot be obtained for any scenario, the solution does not converge. By cutting some slack to the zero mismatch, i.e. by making the equality constraint $mismatch = 0$ an inequality constraint with some level of tolerance, this phenomenon may be avoided. The system and power flow constraints and the mismatch are checked for every hour of every scenario. The blue boxes in Figure. 3.2 represent the loops or the number of times/scenarios the constraints are checked for.

3.1.2 Goal Programming Approach

Another approach that can be used to solve the problem in concern is to treat it with Goal Programming method. As mentioned in section 2.6.1, Goal Programming is a very popular method for solving multi-objective optimization problems. In the block diagram shown in Figure. 3.3, the required steps are shown to solve the problem using Goal Programming.

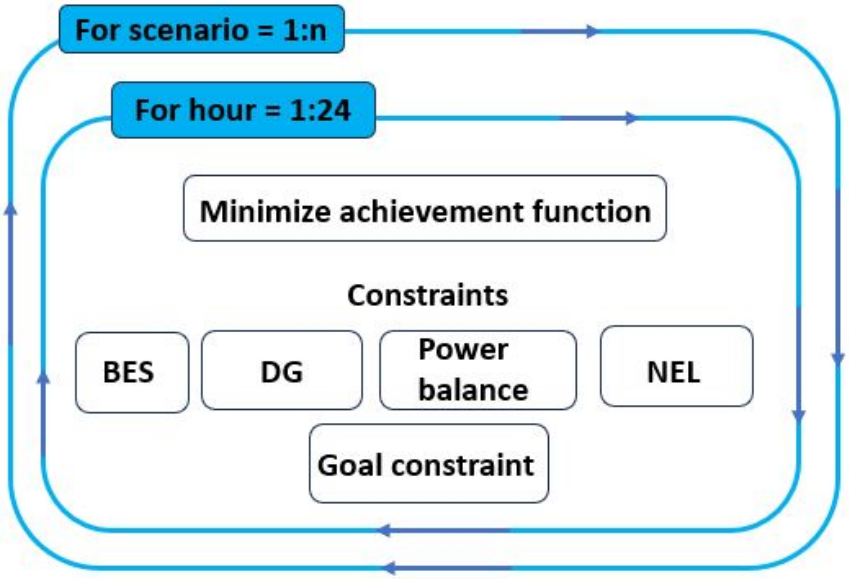

Figure 3.3: Goal Programming Approach

As can be seen, it is also a Single Stage MILP approach. The difference lies in treating the mismatch as an objective function, instead of a constraint, and thus avoiding infeasible solutions.

3.1.3 Decomposition Methods

The Single Stage MLIP may be simple and straightforward in nature, but for a very large number of scenarios it may not converge. To ensure MG resilience, it is necessary to consider thousands of scenarios. Therefore, instead of solving an MILP problem in the centralized manner, a distributed approach is proposed. It is possible to decompose the problem by relaxing the complicating constraints or fixing the

complicating variables as discussed in section 2.8.2.4. However, the aforementioned problem is of complicating variable structure, because it has integer variables (decision variables that represent commitment states of the MG units) which are present in most of the constraints. This makes Bender's Decomposition a suitable candidate to be implemented for decomposing the problem. In Figure 3.4, the Bender's Decomposition approach is presented in steps to solve the concerned problem.

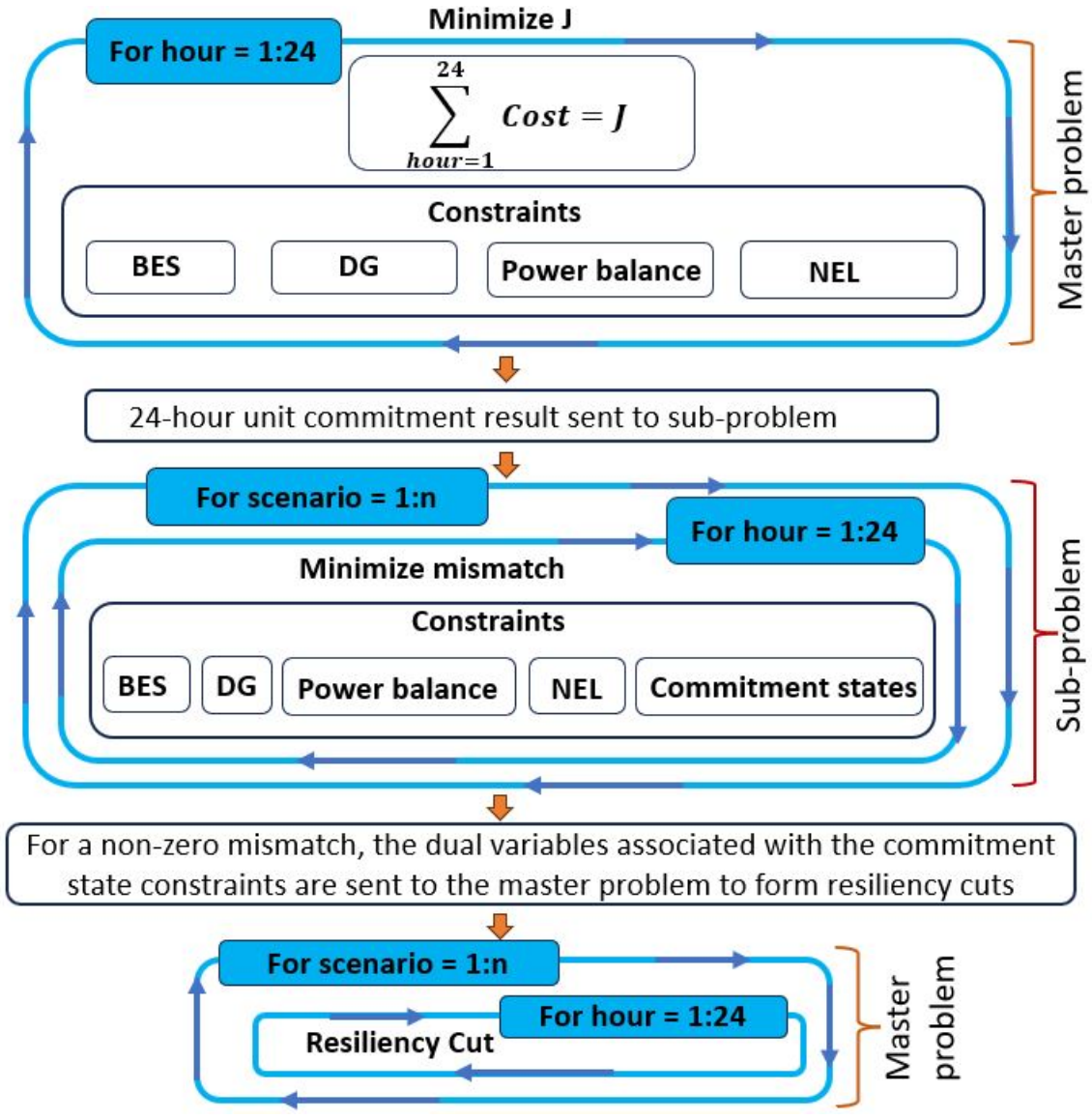

Figure 3.4: Bender's Decomposition Approach

3.2 Proposed Framework - Bender's Decomposition

Using Bender's Decomposition, the original problem is decomposed into a master problem (MP) and a sub-problem (SP) as shown in Figure 3.5.

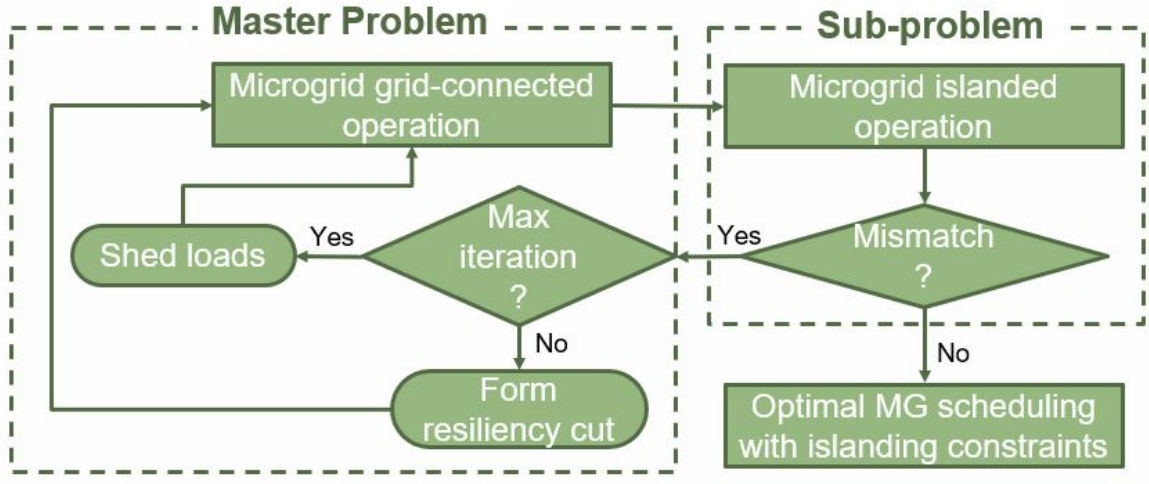

Figure 3.5: The Proposed Framework

It can be seen in Figure 3.4, that the 24 hours unit commitment result is obtained first for the minimum cost. Mismatch is treated as an objective function unlike Single Stage MILP approach, but under a sub-problem unlike the Goal Programming approach. Although the Bender's Decomposition seems more critical compared to Single Stage MILP and Goal Programming approaches, this approach is more beneficial in terms of large number of scenarios, as the original problem is broken down into master problem and sub-problem.

3.2.1 Master Problem

The normal or grid connected operation of the MGs are carried out in the MP, while the resilient operations are handled in the SP. In the MP, the commitment states of the DGs, BES systems and the NEL of all the MGs are determined. These unit commitment states obtained during the normal operation ensure the cost incurred by the MGs is minimum. The results are then sent to the SP. The SP checks for any generation-load mismatch in all possible scenarios in a certain case. Each scenario

has a possibility to have a mismatch for the unit commitment obtained from the MP. If there is no mismatch, the results obtained from the MP are used for scheduling the units. On the other hand, if there is a mismatch in any of the scenarios, the commitment states of the units are revisited in the MP using Bender's cuts or resiliency cuts. The results are then again sent to the SP to check for any mismatch. The process continues until the mismatch is zero for every scenario considered for the event. Load shedding is considered only if there is still a mismatch after the maximum number of iterations has been reached.

3.2.1.1 Cost Function

The maximum benefit of the MGs is ensured by minimizing the power purchased from the grid and operating the least expensive DGs first in all active MGs. The objective function shown in (3.1) aims to achieve this cost minimization. The first portion of the objective function represents cost minimization related to the main grid. The cost (C^G) of purchasing power from or selling power to the main grid is considered to be equal. It is assumed that the MGs cannot simultaneously purchase power from the grid and sell power to the grid. Therefore, the power purchased from or sold to the grid is represented with a single variable (P^G). If power is purchased from the grid, it is considered a generation source for the MGs, therefore P^G is positive. If power is sold to the grid, P^G is negative. The later portion of the objective function minimizes the cost associated with all the DG units in the network. The cost of operating a DG is determined by multiplying the generator fuel cost (C^{DG}) with the power generated (P^{DG}) by, and the commitment state (I^{DG}) of that DG unit.

$$Minimize \sum_{t} \left[(P_t^G C_t^G) + \sum_{i} \sum_{j} P_{t,i,j}^{DG} C_{t,i,j}^{DG} I_{t,i,j}^{DG} \right] \tag{3.1}$$

3.2.1.2 DG Constraints

The maximum and minimum powers that can be drawn from the DGs are restricted using (3.2). The operation of all the DGs are subject to maximum ramp-up and ramp-down limits (3.3,3.4).

$$P_{i,j}^{DG,min} I_{t,i,j}^{DG} \leq P_{t,i,j}^{DG} \leq P_{i,j}^{DG,max} I_{t,i,j}^{DG} \tag{3.2}$$

$$P_{t,i,j}^{DG} - P_{t-1,i,j}^{DG} \leq RU_{i,j} \tag{3.3}$$

$$P_{t-1,i,j}^{DG} - P_{t,i,j}^{DG} \leq RD_{i,j} \tag{3.4}$$

3.2.1.3 Convex Relaxation through McCormick Envelope Method

The aforementioned minimization problem 3.1 and constraint 3.2 have the term $P^{DG}I^{DG}$ in them. Therefore, they are of bilinear NLP by nature. However, the variable I^{DG} is the commitment status of the DG units. Because it is a binary variable, the minimum and maximum will be $I^{DG,min} = 0$ and $I^{DG,max} = 1$ respectively. The problem is then relaxed using the McCormick Envelope method mentioned in section 2.7:

$$Minimize \sum_{t} \left[(P_t^G C_t^G) + \sum_i \sum_j P_{t,i,j}^{DG} C_{t,i,j}^{DG} \right] \tag{3.5}$$

subject to

$$\begin{aligned}
P_{t,i,j}^{DG} &\geq P_{i,j}^{DG,min} I_{t,i,j}^{DG} + P_{t,i,j}^{DG} I^{DG,min} - P_{i,j}^{DG,min} I^{DG,min} \\
P_{t,i,j}^{DG} &\geq P_{i,j}^{DG,max} I_{t,i,j}^{DG} + P_{t,i,j}^{DG} I^{DG,max} - P_{i,j}^{DG,max} I^{DG,max} \\
P_{t,i,j}^{DG} &\leq P_{i,j}^{DG,max} I_{t,i,j}^{DG} + P_{t,i,j}^{DG} I^{DG,min} - P_{i,j}^{DG,max} I^{DG,min} \\
P_{t,i,j}^{DG} &\leq P_{i,j}^{DG,min} I_{t,i,j}^{DG} + P_{t,i,j}^{DG} I^{DG,max} - P_{i,j}^{DG,min} I^{DG,max}
\end{aligned} \tag{3.6}$$

The remaining constraints will not need any relaxation and can be implemented as they appear in the following sections.

3.2.1.4 Power Balance Constraints

The power balance constraint for normal operation is shown in (3.7). This confirms that at a given time, the total generation in the system matches the total load. The total generation in the system includes generation from the main grid (P^G), DGs (P^{DG}), PVs (P^{PV}) and the BESs (P^{BES}). The total load includes power supplied to the essential loads (P^{LD}) and NEL (P^{NEL}).

$$P_t^G + \sum_i \Big[\sum_j P_{t,i,j}^{DG} + \sum_b P_{t,i,b}^{BES} + \sum_k P_{t,i,k}^{PV} \Big] = \sum_i \Big[P_{t,i}^{LD} + P_{t,i}^{NEL} \Big] \quad (3.7)$$

3.2.1.5 Grid constraints

During normal operation, each MG has a maximum limit on how much power to draw from the grid and how much power to sell back to the grid, which is represented by (3.8).

$$-P^{G,max,sell} \leq P_t^G \leq P^{G,max,pur} \quad (3.8)$$

3.2.1.6 Energy Storage Constraints

The charging power supplied to the BES and the discharging power generated by the BES is represented by a single variable P^{BES}. It is assumed that a BES cannot charge and discharge at the same time (3.9). Therefore, when BES is discharging, P^{BES} is positive and a source of generation for the MGs. On the other hand, when charging, P^{BES} is negative and acts as a load. The BESs are charged from the main grid or the MG resources (DGs and PVs).

$$I_{t,i,j}^{dch} + I_{t,i,j}^{ch} \leq 1 \quad (3.9)$$

The maximum power capacity or the charging and discharging limits of the BES systems are expressed in (3.10, 3.11). The maximum energy storage capacity of the BES is presented with SE^{max} (3.12). The charging and discharging of the BES are reflected in the stored energy (3.13).

$$P_{t,i,b}^{BES} \leq P_{i,b}^{dch,max} I_{t,i,b}^{dch} - P_{i,b}^{ch,min} I_{t,i,b}^{ch} \tag{3.10}$$

$$P_{t,i,b}^{BES} \geq P_{i,b}^{dch,min} I_{t,i,b}^{dch} - P_{i,b}^{ch,max} I_{t,i,b}^{ch} \tag{3.11}$$

$$0 \leq SE_{t,i,b} \leq SE_{i,b}^{max} \tag{3.12}$$

$$SE_{t,i,b} = SE_{t-1,i,b} - P_{t,i,b}^{BES} \tag{3.13}$$

3.2.1.7 NEL Constraints

The NEL are adjustable, and therefore have a maximum and minimum limit (3.14). The NEL can be supplied over a period of 24 hours, as long as it is within an acceptable limit, and the total energy adds up to a certain demand for energy (3.15).

$$P_{i}^{NEL,min} I_{t,i}^{NEL} \leq P_{t,i}^{NEL} \leq P_{i}^{NEL,max} I_{t,i}^{NEL} \tag{3.14}$$

$$\sum_{t} P_{t,i}^{NEL} = E_i \tag{3.15}$$

3.2.2 Sub-Problem

To ensure complete resiliency of the MGs during an event, it is essential to guarantee resilient operation for all possible scenarios of that event. The main grid may remain disconnected for prolonged hours. As a result, a power mismatch (m) may occur at any hour in one or more scenarios. The SP objective function ensures that the summation of the mismatches in all the scenarios is minimized (3.16). The total number of scenarios is expressed with Sc. For each scenario, this hourly mismatch

is expressed as the summation of two slack variables - virtual generation (VG) and virtual load (VL) (3.17). The generation and load in the power balance equation (3.18) have to be such that the summation of these variables is zero.

$$Minimize \quad \sum_{s=1}^{Sc} m_{s,t} \tag{3.16}$$

$$m_{s,t} = VG_{s,t} + VL_{s,t} \quad \text{for,} \quad 0 \leq VG, 0 \leq VL \tag{3.17}$$

$$P^{G}_{s,t} I^{G}_{s,t} + \sum_{i} \Big[\sum_{j} P^{DG}_{s,t,i,j} + \sum_{b} P^{BES}_{s,t,i,b} + \sum_{k} P^{PV}_{s,t,i,k} \Big] + VG_{s,t} = VL_{s,t} + \sum_{i} \Big[P^{LD}_{s,t,i} + P^{NEL}_{s,t,i} \Big] + P^{Loss}_{s,t} \tag{3.18}$$

The constraints in (3.9), and (3.2) - (3.14) also apply to the resilient operation problem. During resilient operation, slow charging and discharging rates are considered for all the BES systems to ensure feasible islanding. The unit commitment results (I') obtained from the master problem are assigned to the subsequent variables (I) in the SP to obtain their associated Lagrangian dual multipliers (3.19) - (3.22). These dual variables (α, β^{ch}, β^{dch}, γ) are later used to generate resiliency cuts in the master problem.

$$I^{DG}_{s,t,i,j} = I'^{DG}_{t,i,j}; \quad \text{dual} = \alpha_{s,t,i,j} \tag{3.19}$$

$$I^{dsch}_{s,t,i,b} = I'^{dsch}_{t,i,b}; \quad \text{dual} = \beta^{dch}_{s,t,i,b} \tag{3.20}$$

$$I^{ch}_{s,t,i,b} = I'^{ch}_{t,i,b}; \quad \text{dual} = \beta^{ch}_{s,t,i,b} \tag{3.21}$$

$$I^{NEL}_{s,t,i} = I'^{NEL}_{t,i}; \quad \text{dual} = \gamma^{ch}_{s,t,i} \tag{3.22}$$

3.2.3 Resiliency Cut

The aim is to ensure feasible islanding for all the possible scenarios in an event. After the initial iteration, if there is a mismatch at any hour in any of the scenarios, the

MP will be revised using the resiliency cut shown in (3.23). As can be seen in (3.23), if the hourly mismatch for the given scenario m_s is not zero, the unit commitment state is changed accordingly. The process is repeated until zero mismatch is secured in all possible scenarios.

$$m_{s,t} + \sum_i \Big[\sum_j \alpha_{s,t,i,j}(I^{DG}_{t,i,j} - I^{DG}_{s,t,i,j}) + \sum_b \beta^{dch}_{s,t,i,b}(I^{dch}_{t,i,b} - I^{dch}_{s,t,i,b}) + \sum_b \beta^{ch}_{s,t,i,b}(I^{ch}_{t,i,b} - I^{dch}_{s,t,i,b}) + \gamma_{s,t,i}(I^{NEL}_{t,i} - I^{NEL}_{s,t,i}) \Big] \leq 0 \quad (3.23)$$

3.3 Test System

The algorithm is tested and validated on the modified IEEE 123-bus test system shown in Figure 3.6. Three different layouts of the interconnected MG system are considered to assess the algorithm for various test cases. The first layout (L1) includes all the MGs as pictured in Figure 3.6. The second layout (L2) consists of MG1, MG2 and MG3, whereas the third layout (L3) includes MG2, MG3, and MG4. In all three layouts, the MGs are connected to the main grid via MG2. The system has been modeled using OpenDSS, and power flow and line flow constraints have been verified for each layout and each test case.

3.3.1 MG Resources

Each of the MGs has its own DGs, BES systems, PVs, and NEL as shown in Figure 3.6, and is able to share its resources with the neighboring MGs. In total, there are 7 DGs in all 5 MGs, and each is rated 1000 kW. The solar irradiance and the capacity of each PV is 0.8 kWh/m^2 and 300 kVA respectively. In total, there are fourteen PV panels and six BES systems in the entire system. The maximum power and capacity of each of the BES systems are 600 kW and 1200 kWh, respectively. Each of the MGs has a NEL rated 200 kWh, which can be supplied over the period of 24 hours

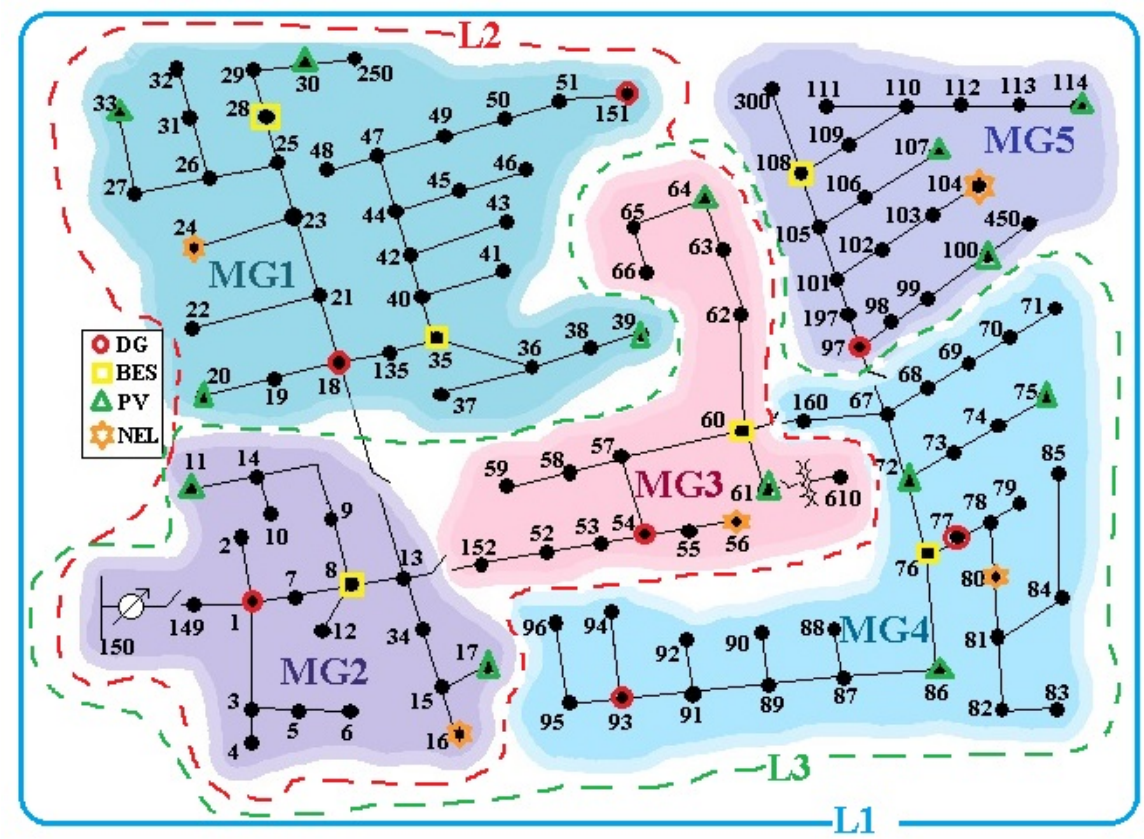

Figure 3.6: IEEE 123-bus test system sectioned into 5 MGs and 3 layouts

within its per-hour maximum and minimum limits. Aside from all the resources, it is assumed that while grid-connected, each of the MG owners can buy back up power or sell excess power back to the grid, subject to a maximum limit. The total load and generation capacity of three different MG layouts are described in Table 3.1.

Table 3.1: Total Load and generation capacity in each layout

MG Layout	Essential Load (kW)	PV (kW)	BES Capacity (kW, kWh)	NEL (kWh)
L1	3310	4480	3000, 6000	1000
L2	1965	2560	2400, 4800	600
L3	1795	2240	1800, 3600	600

Authors considered the 24-hour PV and essential load profile shown in Figure 3.7.

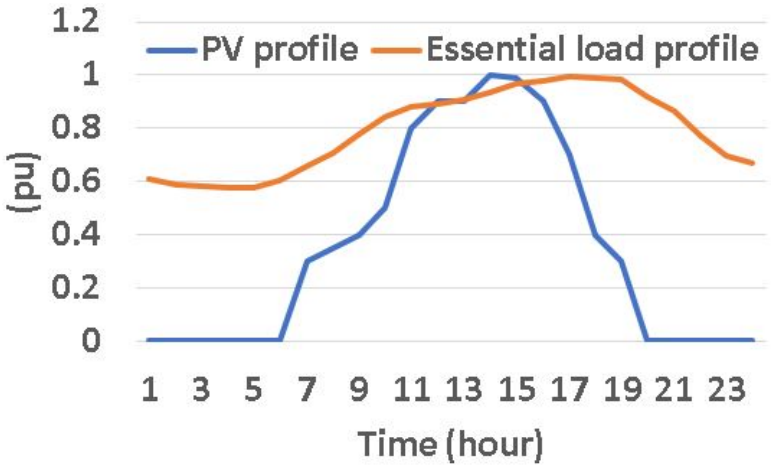

Figure 3.7: Essential load and PV profile

3.3.2 Cost of Resources

The DGs are fueled by natural gas (NG), hydrogen (H_2) and diesel, the cost [118–120] of which are shown in Table 3.2.

Table 3.2: Fuel Costs of the DGs

DG no	MG	Bus no	Commitment State	Fuel	Cost ($/kWh$)
1	1	18	$I_{1,1}^{DG}$	NG	0.25
2	1	151	$I_{1,2}^{DG}$	Diesel	0.34
3	2	1	$I_{2,1}^{DG}$	H_2	0.3
4	3	54	$I_{3,1}^{DG}$	Diesel	0.34
5	4	77	$I_{4,1}^{DG}$	NG	0.25
6	4	93	$I_{4,2}^{DG}$	H_2	0.3
7	5	97	$I_{5,1}^{DG}$	Diesel	0.34

The cost of the main grid energy is $\$0.15/kWh$ [118] during peak hours, and $\$0.13/kWh - \$0.14/kWh$ during off-peak hours. The Levelized Cost of Energy

(LCOE) associated with the PVs account for \$0.12. The battery pack replacement cost is $\$300/kWh$.

3.3.3 Cost of BES and NEL

Even though not included in the formulation, the battery degradation cost is still important to determine. Therefore, this cost is calculated for each BES. The rainflow algorithm is used to calculate the number of cycles from the battery state of charge (SoC). Based on the battery DoD (Depth of discharge) stress model (3.24), the total life loss of the BES is calculated [121]. As shown in (3.25), the total life loss (ΔL) is the sum of the life loss from all cycles. The battery degradation cost (f) is then calculated from ΔL, battery cell replacement cost (B) in $\$/kWh$, and the capacity of battery SE^{max} in kWh, using (3.26). The k_1 and k_2 are battery specific constants empirically fitted to battery life data [122].

$$\Phi(u) = k_1 u e^{k_2 u} \tag{3.24}$$

$$\Delta L = \sum_{l=1}^{N} \begin{cases} \frac{\Phi(u)}{2}, & \text{if } u \text{ is a half cycle} \\ \Phi(u), & \text{if } u \text{ is a full cycle} \end{cases} \tag{3.25}$$

$$f = \Delta L * SE^{max} * B \tag{3.26}$$

During normal operation unit commitment, the NEL is assigned economically throughout 24 hours. However, each of the NEL has an hourly maximum and minimum limit. On top of that, it has to meet a total energy demand throughout this 24-hour period. During resilient operation, even though the maximum and minimum limit on the NEL is still imposed, it may not always meet its total energy demand. In that case, a penalty cost equal to the grid energy price is added to the total cost. In the cost analysis in section 4.1.4, these costs are taken into account.

CHAPTER 4: Results

The optimization problem formulation is done using CVX -a Matlab-based modeling system for convex optimization. The Mixed Integer Linear Programming (MILP) problem is solved using the Gurobi solver. The model is implemented on the modified IEEE 123 bus test system in OpenDSS. The line and system constraints were taken into account, and the losses were included for the power balance constraint. A single machine (A computer with Intel(R) Core(TM) i7-7700HQ CPU @ 2.80GHz processor and 8 GB RAM) has been used for modeling and execution of the proposed method in the benchmark system. The outcomes of this dissertation are categorized into three distinct segments, each elucidated within the corresponding sections of this chapter.

In the first section, the implemented methodology is put to the test within three different layouts of the modified IEEE 123-bus test system. The objective here is to gauge the efficiency and financial implications of optimal scheduling, with a specific focus on determining the advantages of interconnecting multiple MGs versus standalone operation. This comparison serves to highlight the overall benefits of harnessing a network of MGs.

The second section delves into an exploration of the method's sensitivity, specifically concerning the variables of generation and load forecasting errors. This analysis distinguishes between the resilience of a single MG in the face of uncertainties and that of an entire network of MGs. The intention is to showcase how a networked MG infrastructure possesses a distinct advantage in maintaining operational resilience when confronted with varying levels of uncertainty.

Finally, the third section accentuates the superiority of the proposed decomposition method. It does so by drawing a clear comparison between this innovative approach

and the more conventional Single Stage MILP method. The contrast between these two methodologies underscores the unique advantages offered by the proposed decomposition technique.

4.1 Test cases in different multi-MG layouts

The proposed algorithm has been applied in each of the three MG layouts (L1, L2, L3) for three test cases (C1, C2, C3), resulting in nine test cases altogether. In case 1 (C1) and case 2 (C2), the disruption which causes the main grid to be disconnected from the MGs is predicted to occur within a known time frame. The main grid connection status in cases C1, C2 and C3 are shown in Figure 4.1.

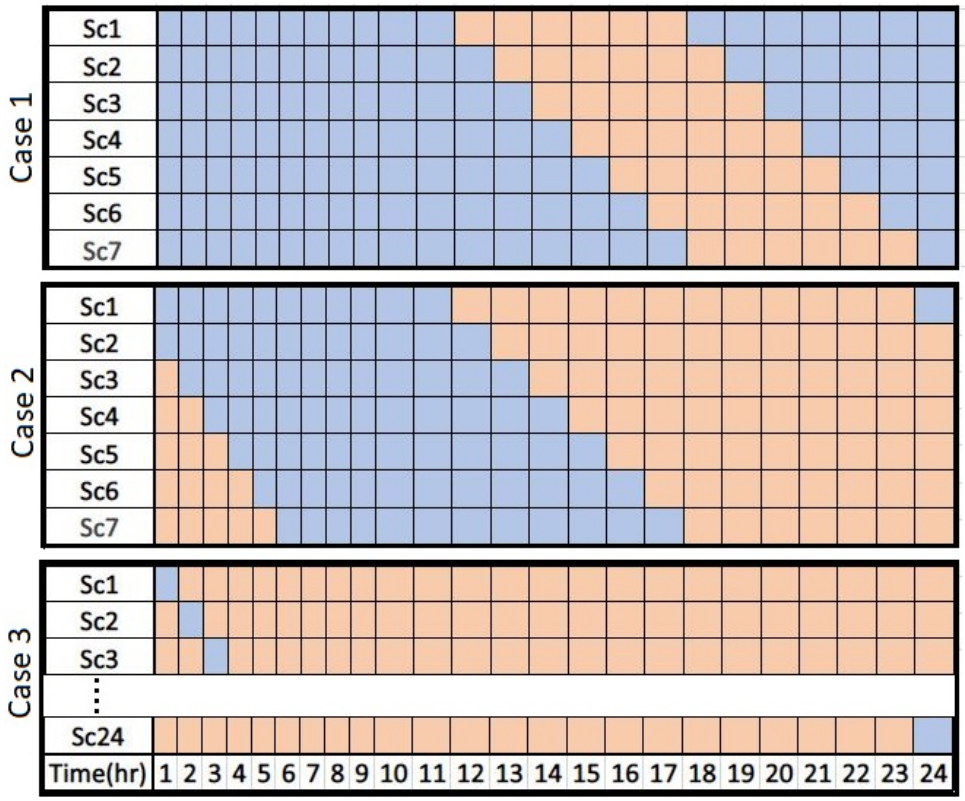

Figure 4.1: Islanding scenarios in cases C1, C2 and C3

The blue boxes are hours of normal or grid connected operation, and the orange boxes reflect the islanding hours. In case C1, it is assumed that the disruption takes place at any hour between $t = 12 - 18hr$, and lasts for 6 hours at a stretch. Similar

to case C1, in case 2 (C2), the islanding is predicted to occur at any hour between $t = 12 - 18hr$. However, in case C2, the islanding lasts for 12 hours at a stretch. In case 3 (C3), an extreme event is considered where the MGs are in risk of being islanded at any hour t, for the next 23 hours at a stretch.

4.1.1 Case 1 (L1C1, L2C1, L3C1)

In case C1, the MGs may get islanded from the main grid at any hour between $t = 12 - 18hr$, and is assumed to remain islanded for the next 6 hours. As a result, there are 7 possible scenarios (Figure 4.1), assuming an islanding scenario for every hour t between $t = 12 - 18hr$. First, the unit commitment is carried out for all the DGs, BES systems, and NEL in the system in the normal operation problem. Later, all the 7 scenarios are checked for any generation-load mismatch in the resilient operation problem. The resilient operation problem returns the hourly mismatch, and the associated dual variables for each of these 7 scenarios which are sent back to the normal operation problem. In the normal operation problem, for each scenario, a resiliency cut is generated to find a solution which satisfies zero mismatch for all the scenarios. If mismatch is not zero, the units are rescheduled in the normal operation problem, and the results are again sent back to the resilient operation problem. The process continues until all the scenarios have zero generation-load mismatch or the maximum number of iterations have been reached. Case C1 is examined for all three MG layouts and are termed L1C1, L2C1, and L3C1. In cases L1C1 and L2C1 the zero mismatch is obtained at iteration-9 and iteration-8 respectively, whereas in case L3C1, it occurs at iteration-5. Among the 7 scenarios in case L3C1, the generation-load mismatch for scenario-1, 3, 5 and 6 at iteration-1, 3, 4, and 5 are presented in Figure 4.2.

As can be seen from Figure 4.2, the unit commitment from initial iteration results in several mismatches throughout the 24 hours in different scenarios. In the subsequent iterations, mismatch is reduced significantly, eventually becoming zero at iteration-

5. It can be observed that scenario-1 and 3 reach zero mismatch at iteration-3, but scenario-5 and 6 still have mismatches at $t = 15hr$. Therefore, the process continues until zero mismatch is obtained for all the scenarios. In Figure 4.3, the commitment states of the DG units are presented at initial and final iteration. It can be observed that even though DG5 was the only DG supplying power at the initial iteration, by iteration-5, DG3 is turned on to reduce the generation-load mismatch in case L3C1. The other 2 DGs in layout L3 (DG4 and DG6) does not need to be turned on while scheduling day-ahead in case C1.

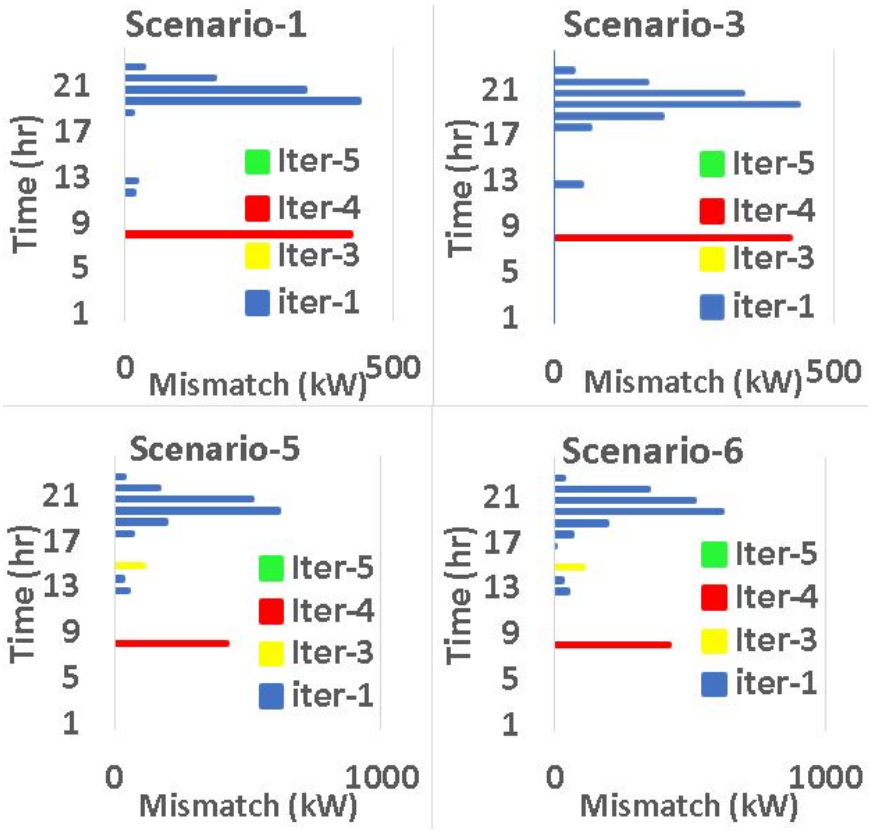

Figure 4.2: Generation-load mismatch for different scenarios in case L3C1 at different iterations

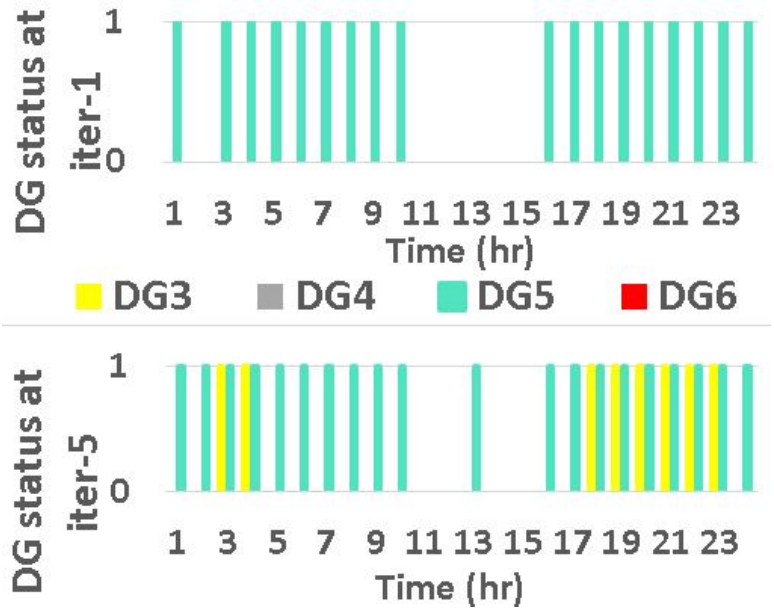

Figure 4.3: DG commitment states in case L3C1 at initial and final iterations

4.1.2 Case 2 (L1C2, L2C2, L3C2)

In case C2, the disruption is predicted to last 12 hours at a stretch. However, the time of islanding is predicted to occur between $t = 12 - 18hr$ like case C1. As a result, case C2 also has 7 scenarios (Figure 4.1) which need to have zero generation-load mismatch. Case C2 is examined for all three MG layouts and are termed L1C2, L2C2, and L3C2. In case L2C2, zero mismatch is obtained for all 7 scenarios at the 5^{th} iteration. Among the 7 scenarios in case L2C2, the generation-load mismatch for scenario-1, 3, 5 and 7 at iteration-1, 3, 4 and 5 are presented in Figure 4.4.

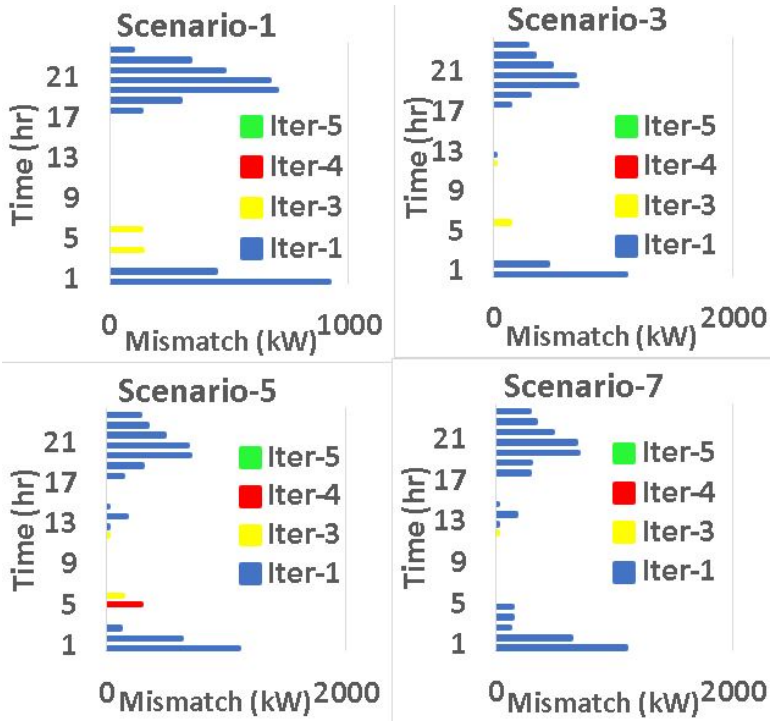

Figure 4.4: Generation-load mismatch for different scenarios in case L2C2 at different iterations

As can be seen from Figure 4.4, the unit commitment from initial iteration results in several mismatches throughout 24 hours in different scenarios. In the next iterations, mismatch is reduced significantly, eventually becoming zero at iteration-5. It can be observed that scenarios-1, 3 and 7 reach zero mismatch at iteration-4, but scenario-5 still has a mismatch at $t = 5hr$. At the 5^{th} iteration, zero mismatch is obtained for all the scenarios. In Figure 4.5, the commitment states of the all 4 DG units of layout L2 are presented at iteration-1 and iteration-5. It can be observed that initially the least expensive generator (DG1) was on, but at the end of the 5^{th} iteration, DG3 is also turned on to minimize the generation-load mismatch. The day-ahead scheduling in case L2C2 does not require the other 2 DGs (DG2 and DG4) to be turned on. However, in cases L1C2 and L3C2, zero mismatch is obtained after the 12^{th} and 6^{th} iterations respectively.

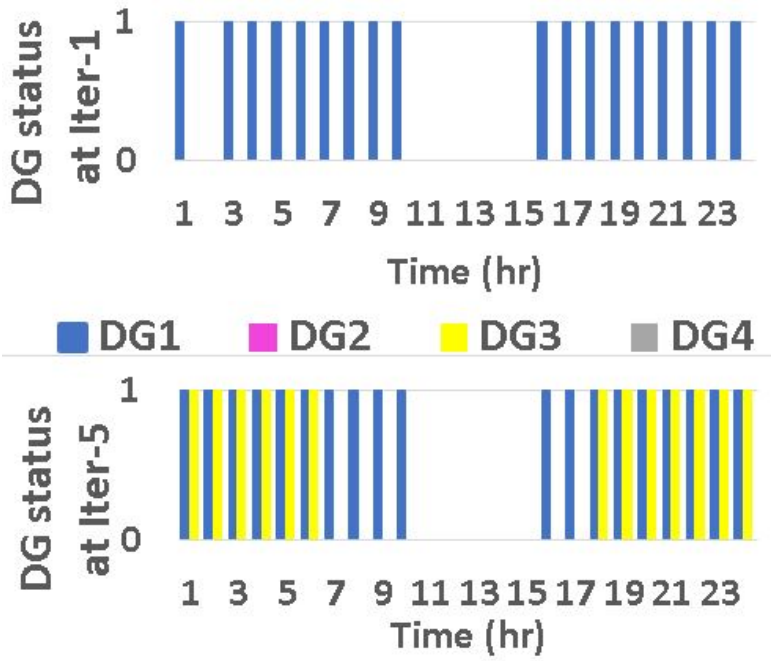

Figure 4.5: DG commitment states in case L2C2 at initial and final iterations

4.1.3 Case 3 (L1C3, L2C3, L3C3)

In case C3, the MGs may get islanded from the main grid at any hour t in the 24 hour period, and is assumed to remain islanded for the next 23 hours. As a result, there are 24 possible scenarios (Figure 4.1), assuming an islanding scenario for every hour t. Case C3 is examined for all three MG layouts and are termed L1C3, L2C3, and L3C3. In case L1C3, zero mismatch is obtained for all 24 scenarios at the 8^{th} iteration. Among the 24 scenarios in case L1C3, the generation-load mismatch for scenario-1, 8, 16 and 22 at different iterations are presented in Figure 4.6. As can be seen from Figure 4.6, the unit commitment from initial iteration results in several mismatches throughout 24 hours in all the scenarios. After that, the mismatch is reduced at every iteration. All but scenario-22 have a zero mismatch at iteration-4, causing the process to continue for 4 more iterations. In Figure 4.7, the commitment states of the all 7 DG units are presented at iteration-1 and iteration-8. 4.6.

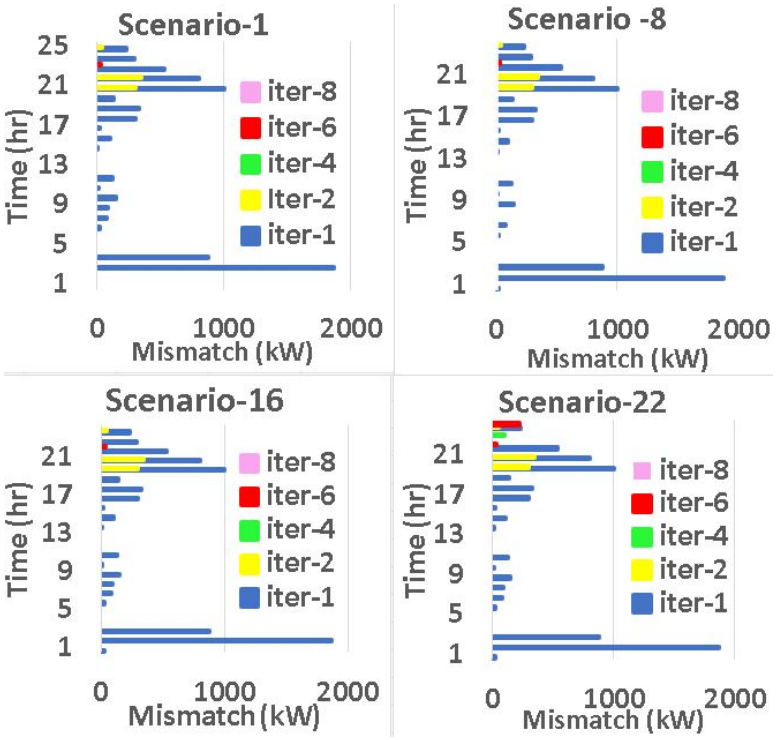

Figure 4.6: Generation-load mismatch for different scenarios in case L1C3 at different iterations

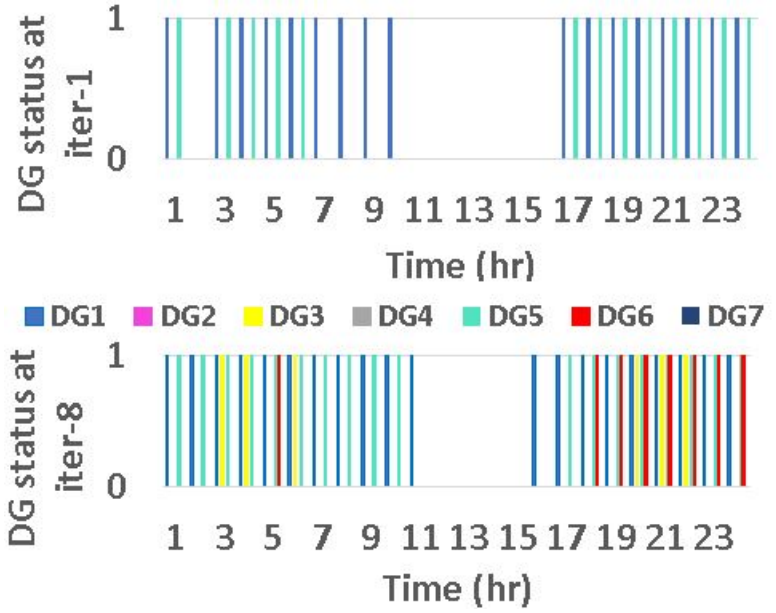

Figure 4.7: DG commitment states in case L1C3 at initial and final iterations

It can be observed that initially the least expensive generators (DG1 and DG5) were on. Later, at the end of the 8^{th} iteration, DG3 and DG6 are also turned on to

minimize the generation load mismatch. Even though case C3 is the most extreme case, the remaining 3 DGs in layout L1 (DG2, DG4 and DG7) do not need to be turned on for day-ahead scheduling in case L1C3. In cases L2C3 and L3C3 the zero mismatches for all 24 scenarios are obtained at iteration-7. The number of variables in the MP, SP, number of iterations and computation time required in each case can be found in Table III. As shown in the table, only the MP has binary variables. A larger number of variables are required in case C3, where 24 SPs are solved for 24 scenarios. The changes of the master problem objective value during the iterations are shown in Figure4.8.

Table 4.1: Number of Variables and Computation Time in each case

Case	No of Scenarios	No of Variables				No of Iterations	Time (s)
		MP Continuous	MP Binary	SP	Total		
L1C1	7	25	24	189	238	9	2335
L1C2	7	25	24	189	238	12	2949
L1C3	24	25	24	648	697	8	6720
L2C1	7	16	15	147	178	8	1362
L2C2	7	16	15	147	178	5	922
L2C3	24	16	15	504	535	7	4286
L3C1	7	14	13	133	160	5	902
L3C2	7	14	13	133	160	6	999
L3C3	24	14	13	456	483	7	3706

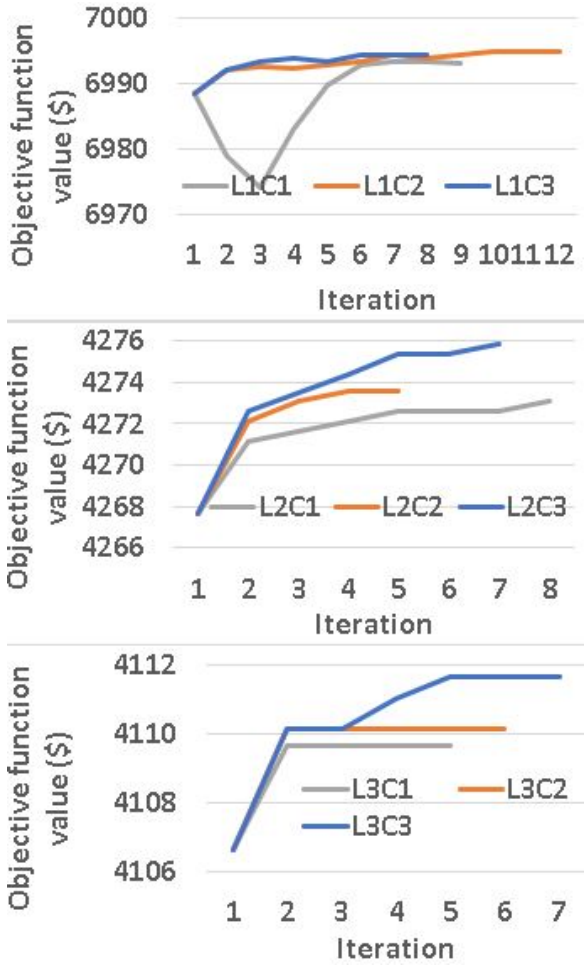

Figure 4.8: The changes of master problem objective value during the iterations

It can be observed from the figure that the general trend of the objective or cost function is to increase with the number of iterations. This is because, when more iterations are needed to reach zero mismatch, the more expensive alternatives are checked. In layout L1, the system has more DG units to choose from. As a result, the objective function or cost increases very slowly (decreases initially in case C1) with the number of iterations. A computer with Intel(R) Core(TM) i7-7700HQ CPU @ 2.80GHz processor and 8 GB RAM has been used to run all the cases.

4.1.4 Cost Analysis

The main goal of this paper was to find the most economic way to schedule the MG units so that the system of MGs is prepared for any event which may cause it to

be isolated from the main grid. In cases C1 and C2, the time of the interruption is predicted beforehand, whereas, in case C3, the islanding is presumed to take place at any hour in the next 24 hours. As the system remains disconnected for 23 hours at a stretch, case C3 is the most extreme situation that the MGs deal with. Islanding at each of these 24 scenarios is considered, and the generation load mismatch is calculated for each scenario. The system loss is taken into account while calculating the mismatch. The power flow and line constraints are implemented, and all the bus voltages remain within the limit.

The final day-ahead scheduling of the DG units for all 9 cases are presented in Table 4.2. The DGs which are absent in the subsequent layout are marked with "X". In section IV, we show that the least expensive generators are turned on first, and the most expensive ones are reserved for the worst case scenarios. From Table 3.2, note that the most expensive DGs are diesel generators, followed by the H_2 generators. The NG generators are the least expensive ones.

Table 4.2: Final commitment states of the DGs for day-ahead scheduling in all 9 cases

	DG1	DG2	DG3	DG4	DG5	DG6	DG7
L1C1	1	0	1	0	1	1	0
L1C2	1	0	1	0	1	1	0
L1C3	1	0	1	0	1	1	0
L2C1	1	0	1	0	X	X	X
L2C2	1	0	1	0	X	X	X
L2C3	1	1	1	0	X	X	X
L3C1	X	X	1	0	1	0	X
L3C2	X	X	1	0	1	1	X
L3C3	X	X	1	0	1	1	X

In Table 4.2, it can be observed that for layout L1, none of the cases require the most expensive DGs or the diesel generators (DG2, DG4 and DG7) to be turned on for day-ahead scheduling. In layout L2, only one (DG2) of the 2 diesel generators (DG2 and DG4) is turned on while scheduling for the most extreme case (C3). Lastly, because layout L3 has only one diesel generator (DG4), and two H_2 generators (DG3 and DG6), DG4 is not required to be turned on in any of the cases. However, both the H_2 generators (DG3 and DG6) need to be turned on sometime in the 24-hour period while scheduling for the most extreme case (C3).

The day-ahead scheduling prepares the MGs to be isolated from the main grid either within a known time frame (C1 and C2), or at any hour t (C3). The costs are calculated for this day-ahead scheduling of the MGs in each case. If the MGs are operated following the day-ahead schedule obtained from the proposed algorithm, the resulting cost of operation for case C3 is presented through the bar chart in Figure 4.9. It can be seen that layout L1 has the highest operating cost, followed by L2 and L3, which is expected given the size of the networks. However, it can also be observed that most of the cost incurred by the MGs is associated with the DGs. The next source of generation contributing to the cost is PV. The grid cost is lower because the MGs have a limit on the maximum backup power they can draw from the grid. The battery degradation cost contributes the least.

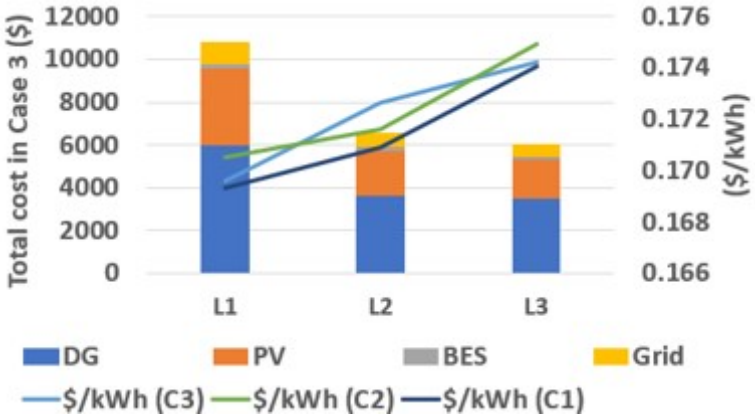

Figure 4.9: Day-ahead scheduling cost comparison among different cases

The lines in Figure 4.9 portray the per unit day-ahead scheduling cost ($\$/kWh$) for all 9 cases. The black, green, and blue lines represent the costs in cases C1, C2 and C3 respectively. As can be observed, the per unit cost is the least for layout L1, and the highest for layout L3. This can be explained from Figure 4.10, where it is shown that the ratio of the PV vs total load of the system is the lowest in layout L3.

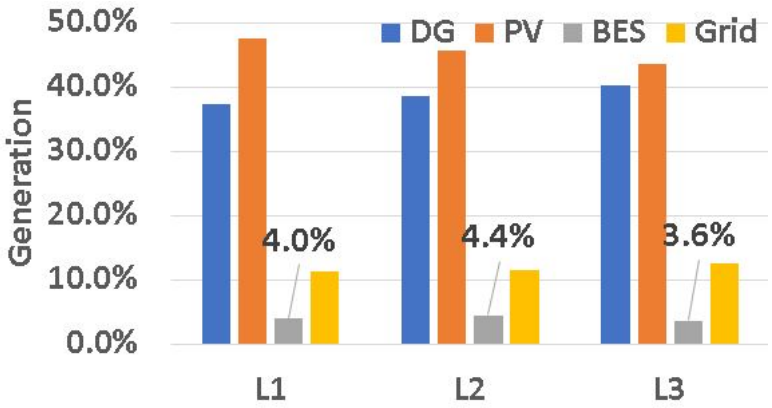

Figure 4.10: Percentage of generation from each type of source in layouts L1, L2 and L3

As PV is less expensive than the DGs, the per unit cost of layout L3 becomes higher than those of L1 and L2. This also emphasizes the importance of resource sharing in the multi-MG network both in terms of resilience and cost saving.

Also, the cost of day-ahead scheduling layouts L1 and L3 for case C3 is lower than that of C2. This is because the battery degradation cost is higher in layouts L1 and L3 for case C2. Because battery degradation cost depends significantly on the number of cycles, and the 12 hour outage scenario demands the battery to perform more cycles, the cost is higher. However, that is not the case with layout L2. This is because L2 has more active power from the BES than layouts L1 and L3, as can be seen in Figure 4.10. The battery degradation cost and the penalty cost for shifting the NEL are not considered within the objective function but are added later for cost comparison. Therefore the scheduling decision does not depend on these two costs. On another note, the costs associated with the resilient operation during various scenarios are also

presented in Figs. 4.11 -4.13. In Figure 4.11, the costs of operating layout L1 in the resilient mode for the 7 scenarios (Sc1- Sc7) in cases C1, C2, and the first 7 scenarios in case C3 are presented. The cost of operating layouts L2 and L3 in the resilient mode for those scenarios are presented in Figure 4.12 and Figure 4.13 respectively. It can be seen from all three figures that the MGs incur the highest cost in the most extreme situation (C3), and it remains quite stable throughout the scenarios. The costs for cases C1 and C2 tend to increase as the scenarios move from scenario 1 to scenario 7. This is because unlike case C3, the MGs are not islanded at any hour and does not remain islanded for more than 12 hours. As the islanding scenario moves towards the later part of the day when the PV has no output, the cost of operation increases.

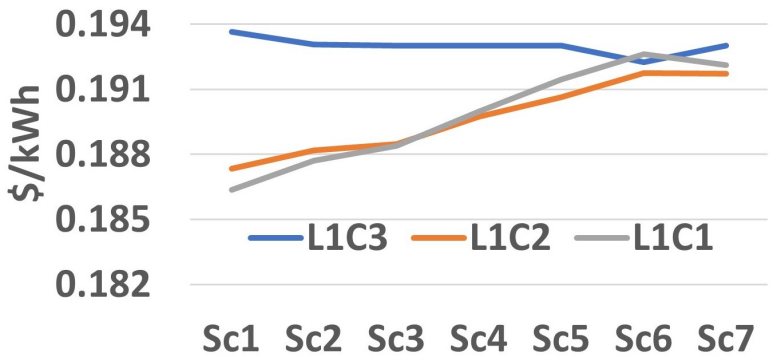

Figure 4.11: Cost of resilient operation in layout L1

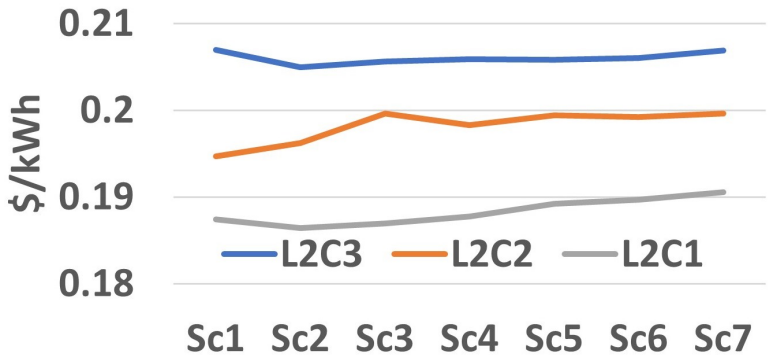

Figure 4.12: Cost of resilient operation in layout L2

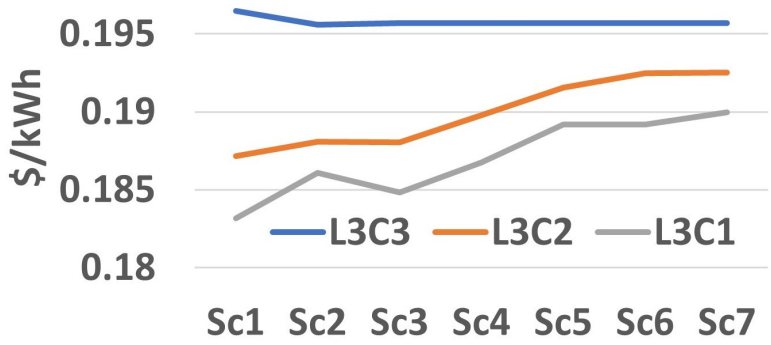

Figure 4.13: Cost of resilient operation in layout L3

4.2 Sensitivity to uncertainty

The sensitivity to uncertainty or forecasting error is presented in Figure 4.14. The amount of load shedding (kWh) required to take place in L1C3 for a load forecasting error (LFE) and/or a generation forecasting error (GFE) are shown in Figure 4.14. The LFE/GFE is calculated by subtracting the actual load/PV generation from the forecasted load/PV generation. Therefore, if the forecasted load/generation is higher than the actual, the LFE/GFE is positive, and if lower then LFE/GFE is negative. Because load shedding is required only if the actual load is higher or the actual generation is lower than what has been forecasted, only the negative LFE and positive GFE are portrayed in Figure 4.14.

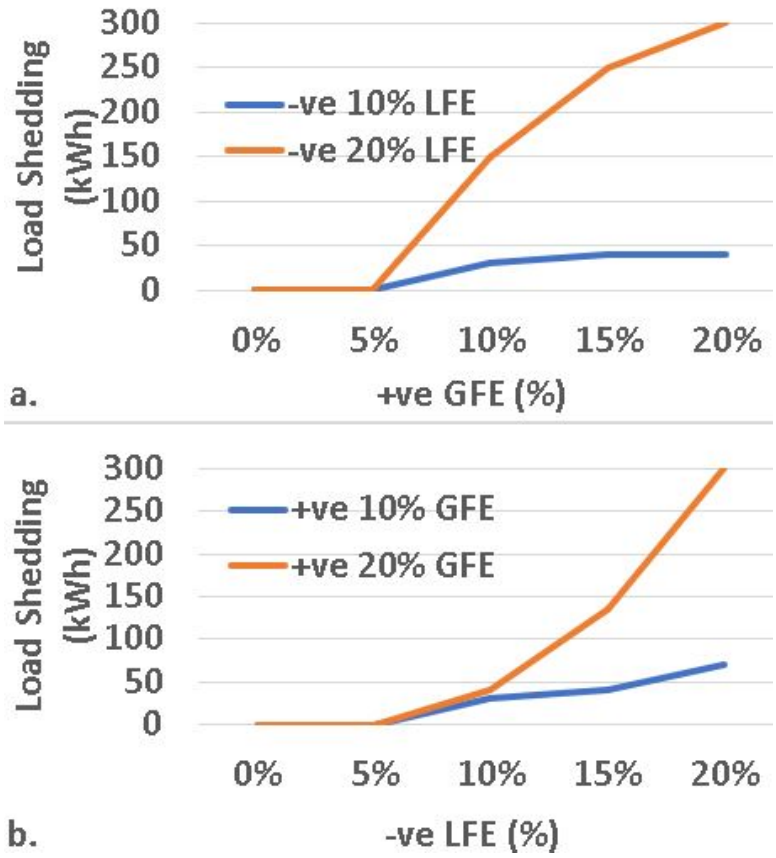

Figure 4.14: Sensitivity to forecasting error in L1C3

In Figure 4.14a., the LFE is fixed at 10% (blue line) and 20% (red line) as the GFE is varied along the x-axis between 0-20%. In Figure 4.14b., the GFE is fixed at 10% (blue line) and 20% (red line) as the LFE is varied along the x-axis between 0-20%. It can be seen from both the figures that load shedding is required for LFE/GFE greater than 5%. In Figure 4.14a., at 10% GFE, the required load shedding increases from 40 kWh to 150 kWh if the LFE is increased from 10% tp 20%. At 15% GFE, the required load shedding increases from 45 kWh to 250 kWh. On the other hand, In Figure 4.14b., at 10% LFE, the required load shedding is almost the same (40 kWh) for 10% or 15% GFE. Again, at 15% LFE, the required load shedding increases from 50 kWh to 120 kWh for a 10% change in the GFE. Therefore, it can be concluded that the system is more sensitive to load forecasting error than to generation forecasting error.

A comparison of the proposed multi-microgrid formulation with single microgrid formulations is shown in Figure 4.15 below.

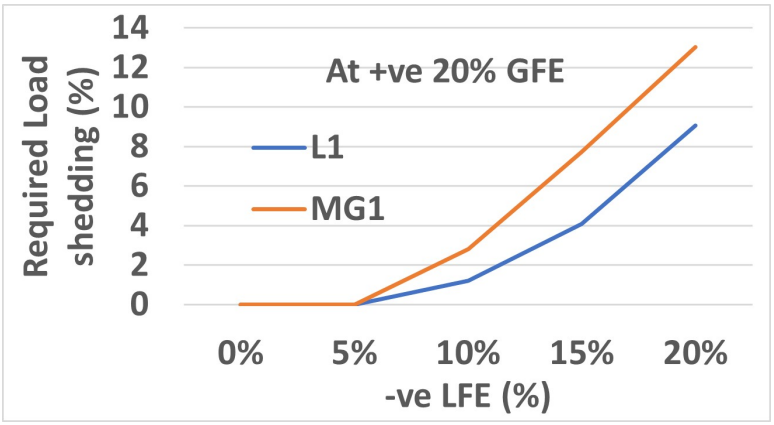

Figure 4.15: Comparison between L1 and MG1 of required load shedding

In the proposed layout, denoted as L1, there are five networked MGs. In contrast, the single MG structure, represented by MG1, consists of just one isolated microgrid. Now, when the actual PV generation falls short by 20% compared to what was initially forecasted (resulting in a positive GFE), the situation presents a stark contrast between the two scenarios.

In the single MG context, where only MG1 is in operation, the magnitude of load shedding required is notably higher. This means that in the event of a GFE, the single MG scenario experiences more significant load curtailment to align with the reduced PV generation, leading to greater disruptions.

Conversely, in the multi-MG scenario (L1), where five interconnected MGs collectively manage the power resources, the impact of the negative LFE is less severe. Despite facing increasingly unfavorable LFE conditions, the interconnected MGs can distribute and manage the load more efficiently, mitigating the need for extensive load shedding and minimizing disruptions. This highlights the advantage of networked MG structures in handling fluctuations in renewable energy generation

4.3 Comparison between Bender's Decomposition and Single Stage MILP approach

The problem at hand has been solved for the entire layout of 5 MGs (L1) using both Bender's Decomposition and Single Stage MILP methods. Given that the islanding state of the MG is binary for every hour, this translates to a vast number of potential scenarios over the next 24 hours. Specifically, there are 2^{24} possible combinations, which amounts to a staggering 16,777,216 scenarios. To provide a meaningful comparison of computational efficiency and solutions, a subset of random scenarios has been selected from this multitude. These selected scenarios offer insights into the performance of both the Bender's Decomposition and Single Stage MILP approach.

4.3.1 Comparison of computational time

The number of scenarios considered indeed exerts a significant impact on computational time, as the number of variables escalates in tandem with the number of scenarios (as outlined in Table 4.1). To provide a comprehensive perspective, a wide spectrum of scenarios has been taken into account for this comparative analysis. The computational time has been meticulously documented as the number of scenarios is incrementally doubled or closely approximated. The comparison encompasses scenarios ranging from a minimum of 6 up to a maximum of 1000 scenarios, and the results are visually presented in Figure 4.16.

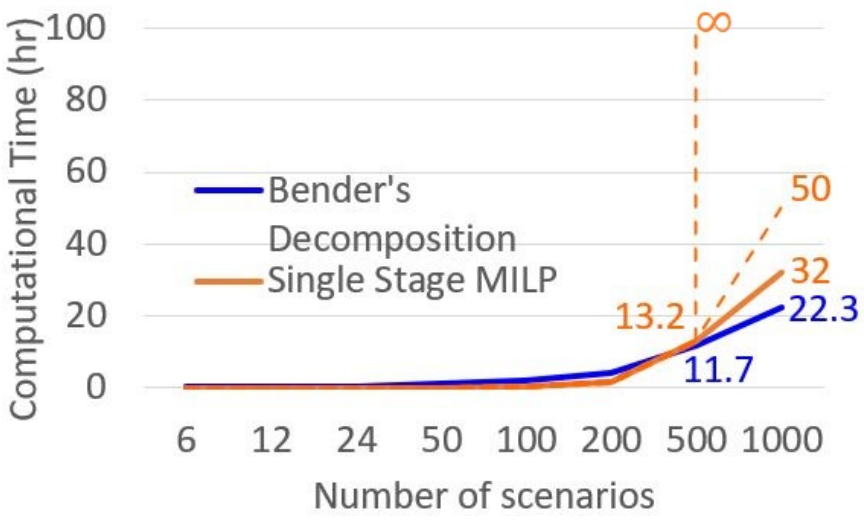

Figure 4.16: Comparison of computational time

In Figure 4.16, the computational time taken to solve the problem is shown along the y-axis. In the x-axis, the number of scenarios are presented. It can be noticed that for up to 200 number of scenarios, it takes more time to solve the problem using Bender's Decomposition than it does using Single Stage MILP approach. When the number of scenarios considered is increased to 500, the computational time becomes less for the Bender's decomposition than for the Single Stage MILP approach. It takes 11.7 hours to solve the problem for 500 scenarios using Bender's Decomposition method, whereas it takes 13.2 hours to solve it using Single Stage MILP approach.

To further justify the use of decomposition technique, the number of scenarios are increased to 1000. As can be seen in Figure 4.16, the problem is solved in 22.3 hours when Bender's Decomposition technique is used. However, when Single stage MILP approach is used, no solution is obtained at least til 32 hours. It is possible that the solution is reached after that, or it never converged. So, it can be concluded that the solution of this problem if at all obtainable using Single stage MILP approach, takes longer than 32 hours. The comparison for smaller number of scenarios can be observed better from the Table 4.3.

In Table 4.3, the computational time and the obtained solution are compared be-

tween the Bender's Decomposition and Single Stage MILP approaches. It is shown that even though the solution or the optimal cost is quite close if not the same for both the approaches, the computational time varies significantly. For small number of scenarios, the Single Stage MILP approach performs remarkably better. In Bender's Decomposition, the computational time doubles with doubling the number of scenarios. However, as the number of scenarios doubles, the computational time in Single stage MILP approach increases even at a faster rate, eventually exceeding the time taken by the Bender's Decomposition approach.

Table 4.3: Solving time and optimal solution obtained from Bender's Decomposition (BD) and Single Stage MILP (SMILP) methods

No of scenarios	Computational time (hour)		Optimal cost ($)		No of iterations in BD
	BD	SMILP	BD	SMILP	
6	0.22	0.01	6931.5	6931.5	9
12	0.25	0.02	6954	6954	6
24	0.55	0.04	6931.5	7003.5	5
50	1.01	0.13	7003.5	7003.5	6
100	2.14	0.39	7003.5	7003.5	6
200	4.16	1.45	7003.5	7003.5	6
500	11.7	13.21	7003.5	7003.5	6
1000	22.33	>32	7003.5	7003.5	6

It is worth mentioning that all the cases presented in Table 4.3 have been solved using the same machine (Personal laptop) and under the same computing environment. A mini, mainframe, super-computer or even a personal computer will have a much faster computational time. However, those machines will result a faster run-time for both the approaches. Therefore, using the same machine for all the computations makes the comparison completely reliable.

4.3.2 Comparison of solutions

Even though the computational time is significantly different for the two approaches, the optimal solution is very close, if not same to each other, as shown in the fourth and fifth column of Table 4.3. In the right most column, it shown that it may take anywhere between 5-9 iterations to reach the solution when Bender's Decomposition technique is applied. At each iteration, a new Bender's cut is introduced to mitigate the non-zero mismatch which occurs at the previous iteration. However, after the final iteration, the obtained solution matches with the solution obtained from the Single Stage MILP approach.

In Bender's Decomposition, an optimal objective function or optimal cost is obtained for every iteration until the final iteration where the zero mismatch is obtained. In Figure 4.17, those optimal costs are shown for scenarios 6, 12, 24, 50 and 1000. The number of iterations are shown in x-axis, while the optimal cost is shown along the y-axis. It can be observed that in all the scenario types, the first iteration starts with the same objective value, which is the cost of operation when no islanding scenarios are to be satisfied. However, as the number of scenarios increase so does the optimal cost. For scenarios 6, 12 and 24 the optimal cost does not increase after the second iteration. However, for scenarios 50 and 1000, the optimal cost increases after the fifth iteration. This is understandable as the more number of scenarios exhaust more scheduling options. Also, the 12 scenario case takes more iterations to solve and results higher optimal cost than 24 scenario case. This is purely due to the random nature of the scenarios.

The optimal function values obtained through the Single Stage MILP approach is shown with "$*$". Because there is no iteration involved in the Single Stage MILP process, the optimal objective function values are shown along zero iteration. It is evident from Figure 4.17, that the optimal costs obtained from the Single stage MILP approach mathces the optimal cost obtained at the final iteration through Bender's

Decomposition method in most of the cases. The only exception being the 24 scenario case, where the optimal cost function is higher when sought through Single stage MILP approach.

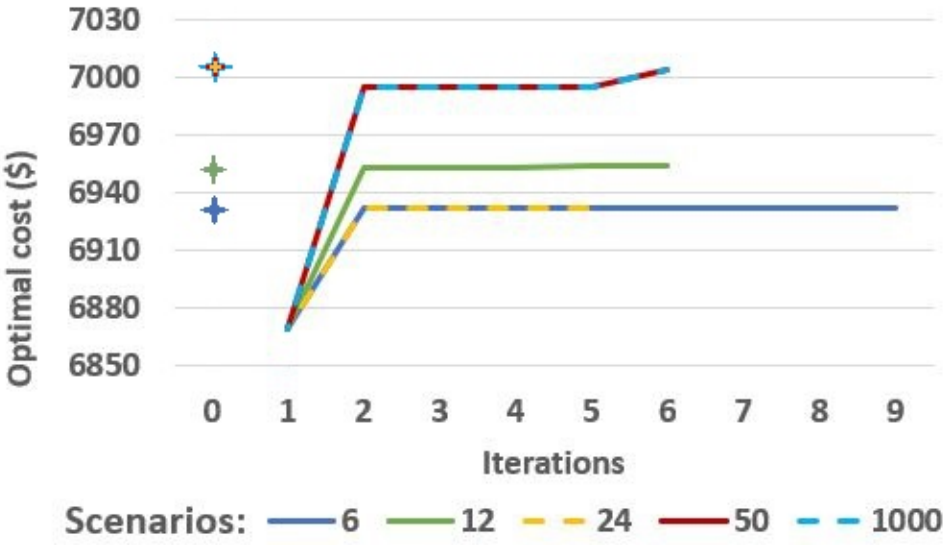

Figure 4.17: Optimal cost comparison with Single Stage MILP approach and different iterations in Bender's Decomposition approach

It can be observed from Table 4.17 and 4.17, that for the 24 scenarios, the optimal cost achieved through Bender's Decomposition is slightly lower than the optimal cost obtained through SMILP approach. Because the cost is largely dependent on the operational cost of the DG units, the optimal scheduling of the DGs for 24 scenario case found through both the approaches are presented in Figure 4.18.

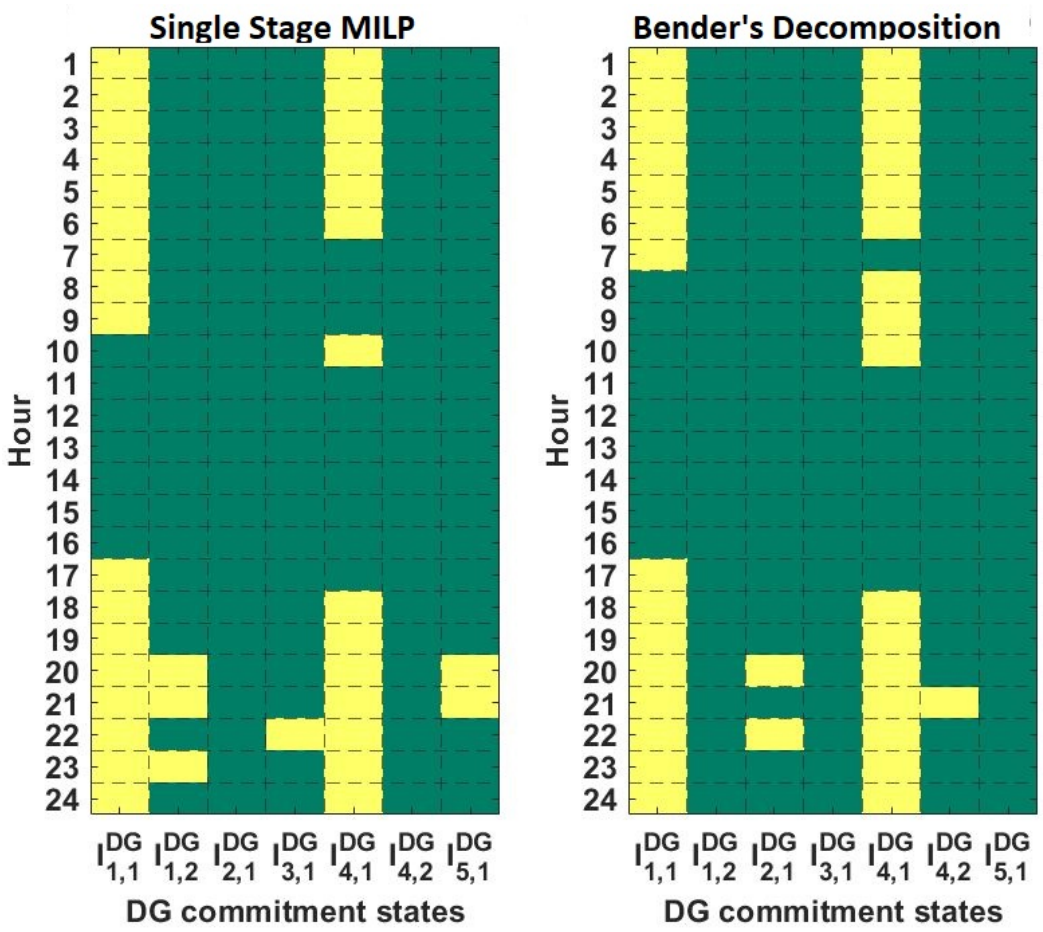

Figure 4.18: Optimal DG commitment states ($I^{DG}_{i,j}$) using Single Stage MILP and Bender's Decomposition method in the 24 scenario case

As mentioned in Table 4.3, the solution is obtained after the fifth iteration of the Bender's Decomposition method. Therefore, the DG scheduling shown on thr right side of Figure 4.18 is obtained after the fifth iteration of the Bender's Decomposition method. On the left-side, the optimal DG scheduling for 24 scenarios obtained from the Single Stage MILP approach is presented. The green blocks mean the commitment state is "on" or "1", while the yellow block means the DG commitment state is "off" or "0". It can be observed that commitments states $I^{DG}_{1,1}$ and $I^{DG}_{4,1}$ are "1" longer than the others. This is expected, as those 2 DGs (DG1 and DG5) are the least expensive (Table 3.2. Also, the Diesel generators (DG2, DG4 and DG7) are the most expensive ones. As a result, the optimal scheduling through Bender's Decomposition results "0"

for those commitment states ($I_{1,2}^{DG}$, $I_{3,1}^{DG}$ and $I_{5,1}^{DG}$). Using Single stage MILP approach yields an optimal scheduling that sugges turning on those DGs for couple of hours. As a result, the optimal cost is a bit higher for Single stage MILP approach than Bender's Decomposition method (Table 4.3).

On another note, it can be observed in Table 4.17 that the optimal cost of day ahead scheduling for 24 scenarios is less than that of 12 scenarios. This is an indication that the optimal cost does not necessarily increase with the number of scenarios considered, but the type of scenarios. The optimal cost increases only when certain scenarios force the more expensive DGs to be turned on. Similarly, the number of iterations required by the Bender's Decomposition technique, before it returns a solution also depends on the type of scenarios, rather than the number of scenarios. That is why it is possible to obtain a solution for 1000 scenarios in only 6 iterations, while it takes 9 iterations to obtain a solution for 6 scenarios (Table 4.17).

The optimum DG commitment states obtained through Bender's Decomposition method for 6 scenarios from iteration-1 and iteration-9 is shown in Figure 4.19. It can be observed that at iteration-1, only DG1 and DG5 (commitment states $I_{1,1}^{DG}$ and $I_{4,1}^{DG}$ respectively) are turned on. However, by iteration-9, DG3 and DG6 (commitment states $I_{2,1}^{DG}$ and $I_{4,2}^{DG}$ respectively) are also turned on to eradicate any mismatch in those 6 scenarios.

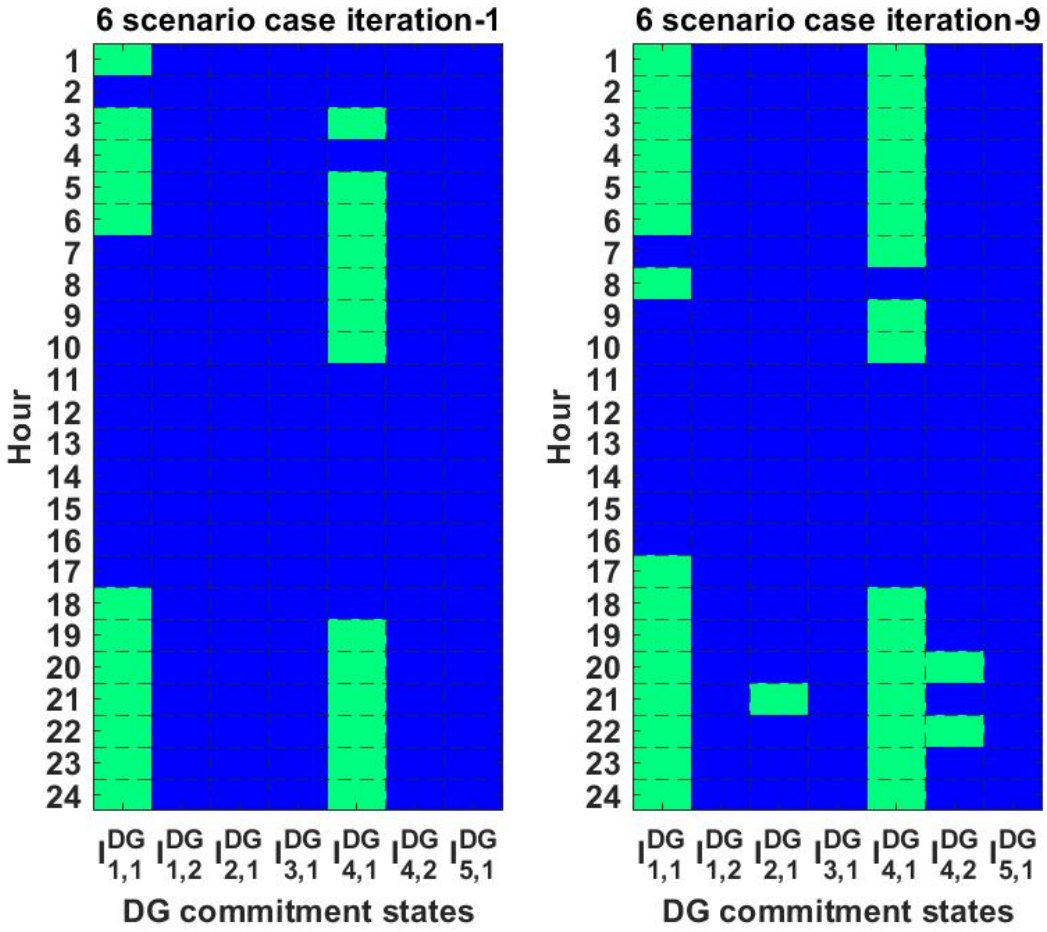

Figure 4.19: Optimal DG commitment states ($I^{DG}_{i,j}$) at iteration-1 and iteration-9 using Bender's Decomposition in the 6 scenario case

Even when the final optimal cost is same in most cases, the resulting optimal scheduling may be different for Bender's Decomposition than the Single Stage MILP method. For instance, the optimal DG commitment states obtained through both the methods for 50 scenarios case are presented in Figure 4.20. It can be observed that $I^{DG}_{1,2}$, and $I^{DG}_{3,1}$ (Commitment states of DG2 and DG4) are turned on for a longer duration in the Single stage MILP approach than in Bender's Decomposition approach. On the other hand, $I^{DG}_{5,1}$ (DG7) is never turned on in Single stage MILP approach, but turned on for 3 hours in Bender's Decomposition approach. Because all these DGs are more expensive compared to DG1 and DG5, different combinations of them can yield the same optimal result.

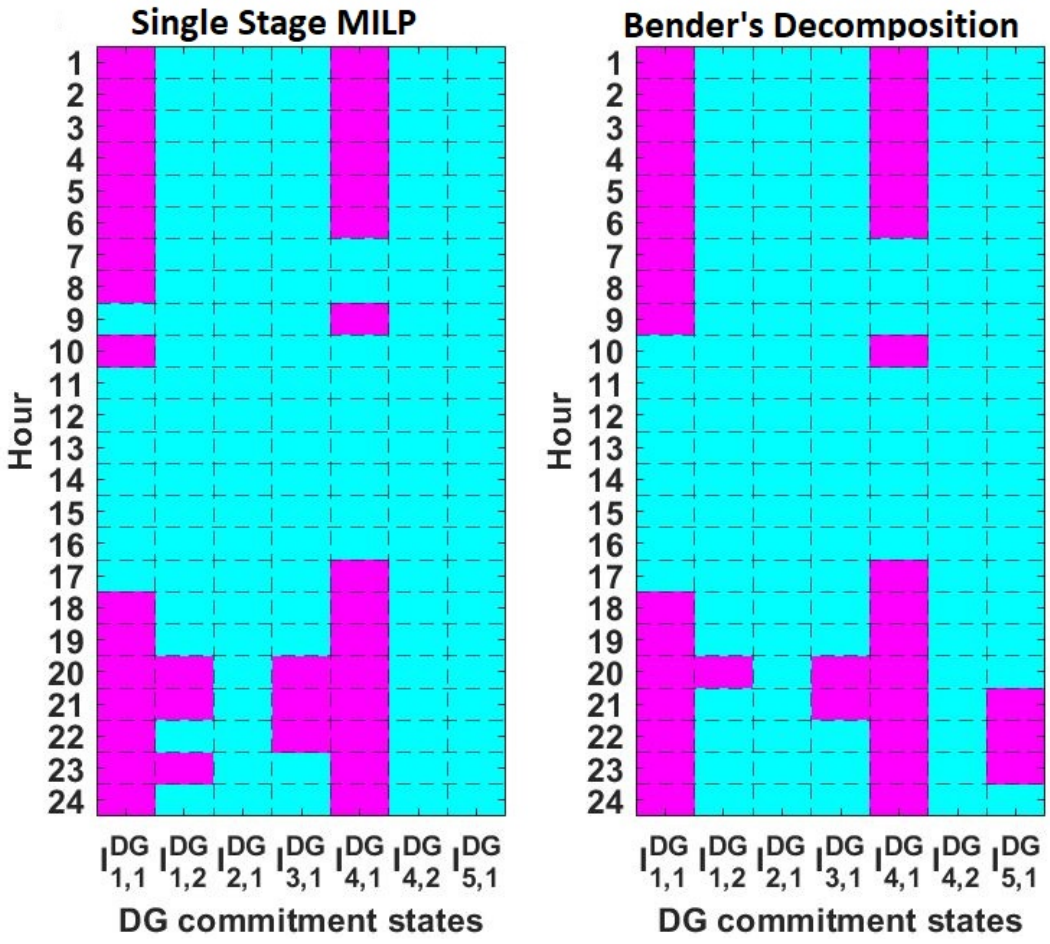

Figure 4.20: Optimal DG commitment states ($I_{i,j}^{DG}$) at for 50 scenarios using Single Stage MILP and Bender's Decomposition method

As mentioned earlier, in order to ensure zero mismtach for every scenario, some non-essential loads may be rearranged across the 24 hour time period. As long as the total energy offered to the customers are met over the period of 24 hours, a penalty is added to the cost for any inconvenience caused for this rearrangement. However, this penalty is added after the optimal cost is determined. Therefore the non-essential loads do not have any direct affect on determining the optimal objective function. However, they do play an essential role in mitigating mismatch. This can be observed in Figure 4.21.

Hour	Single Stage MILP approach (kW)					Bender's Decomposition (kW)				
	P_1^{NEL}	P_2^{NEL}	P_3^{NEL}	P_4^{NEL}	P_5^{NEL}	P_1^{NEL}	P_2^{NEL}	P_3^{NEL}	P_4^{NEL}	P_5^{NEL}
1	10				10	50	50	50	50	50
2						50	50	50		50
3			10				50	50	50	
4				10						
5		10			10				20	
6						20			10	
7	10		10							
8	10	10	10	50	10					
9						50				
10	10	10	10	10	10			20		
11	50	10	10	50	50					
12	10	10	10	10	10					
13	10	10	10	10	50		10			
14	10	10	10	10	10					
15	10	10	10	10	10					
16	50	10	10	10	10			10		
17	10	10	10	30	20					
18		40	50				20		10	30
19										50
20						10	10		50	
21	10					10	10	10	10	10
22		10	40							
23						10				
24		50						10		10

Figure 4.21: Optimal NEL scheduling obtained through Single Stage MILP and Bender's Decompsiotion approach

In Figure 4.21, the NEL scheduling obtained through Single stage MILP approach and Bender's Decomposition methods are shown for 500 scenarios. The grey areas are when the loads are not in schedule. For the remainder of the hours, the scheduling is bounded by the maximum of 50 kW/hour and minimum of 10 kW/hour (3.14). Also, in accordance with 3.15, the total energy for each NEL sums up to 200 kWh. It is interesting to see that in the SMILP approach the loads are scheduled more towards middle of the day, where as in Bender's Decomposition approach they are spread out more towards the beginning or end of the day.

CHAPTER 5: Conclusions

The idea of networking multiple MGs has been in practice for quite some now. Leveraging this technological advancement to obtain absolute resiliency and maximum economic benefit is a newer challenge. This dissertation proposes a novel method to address the utility of networking multiple MGs in securing resilient operation through day-ahead scheduling. Achieving the optimal operational cost is also significant besides ensuring resilient operation. Therefore, this research also incorporates cost comparison among multiple MG layouts to determine economic benefit of connecting multiple MGs during extreme events. The primary focus of this dissertation is to address the challenges related to uncertain MG islanding scenarios, particularly in the context of unfavorable events. It aims to provide a robust solution to the optimal day-ahead scheduling problem in these scenarios. The innovative model proposed in this study is not only unique but also highly adaptable. One of its notable features is modularity, which allows for the seamless integration of new MGs and their various components.

An essential aspect of this model is its decomposition technique, which enhances its practicality for centralized MG optimization while effectively managing computational complexity. First, the original multi-objective MILP problem of minimizing the operating cost as well as the generation-load mismatch is identified as decomposable in nature. Thus, the problem is decomposed into a master problem that deals with cost minimization, and sub-problems that minimize the mismatch in different possible scenarios. This decomposition technique, known as Bender's Decomposition involves a number of iterations until zero mismatch is obtained for all scenarios being considered. For any mismatch in an iteration, the initial unit commitment results

obtained from the master problem is revised using Bender's cuts.

As opposed to the proposed decomposition technique, the more straight-forward way to solve the problem is following the Single Stage MILP approach. To avoid the complexity of a multi-objective problem, the objective of minimizing the generation-load mismatch is presented as a constraint instead. The number of variables remain the same as the Bender's Decomposition method, and there is no need for multiple iterations. The problem is solved as a single large problem.

Initially, the implementation of Bender's Decomposition in single MG optimal scheduling yielded promising results, showcasing the model's potential. However, the true novelty of this research lies in its extension to MG clusters, making it possible to apply this approach within a widely-accepted benchmark system. The model is applied and evaluated on the modified IEEE-123 bus test system, divided into 5 MGs. All together, there are 7 DGs, 6 BES systems and 14 PVs acting as local power sources of these 5 MGs (layout-1 or L1). During normal operating condition, generation from the DGs, PVs, BES systems and the main grid account for 37.3%, 47.4%, 4% and 11.3% respectively of the total load in L1. In L2 there are 3 MGs (MG1, MG2, M3) consisting of 4 DGs, 4 BES systems and 8 PVs supplying 38.5%, 45.6%, 4.4% respectively of the total load while grid connected. Lastly, L3 also consists of 3 MGs (MG2, MG3 and MG4). During normal operation, the 4 DGs, 3 BES systems and 7 PVs in L3 supply 40.2%, 43.7%, 3.6% of the total load respectively. While the total essential load in L1, L2, and L3 are 3310 kW, 1965 kW and 1795 kW respectively, there is a 200 kWh of non-essential load in each layout. While implementing the model in different layouts of the test system, the system and line constraints are taken into account. In addition, the line and system losses are considered while calculating power mismatch.

In addition to proposing the decomposition method for effectively and economically preparing the MG network for such events, the research also compares it with

the traditional Single Stage MILP approach. The proposed method has shown better computational performance for larger number of scenarios during an event, which is more practical to ensure resilient operation.

5.1 Result Analysis

The analysis of the results highlights a notable trend where, in the majority of cases, the most expensive DGs remain inactive during the various islanding scenarios. This intriguing observation suggests a cost-effective and environmentally beneficial approach to managing the MG's power generation. It's worth noting that the diesel generator is only activated in the layout L2 configuration during the most extreme event (C3). This judicious utilization of resources not only optimizes costs but also contributes to a reduction in the ecological footprint.

However, it's essential to acknowledge that certain factors, if considered, could introduce some variations in the results. Elements such as the initial SoC of all BES systems, the initial commitment state and generation of all DGs, and other relevant variables may exert influence on the day-ahead scheduling decisions. These nuanced considerations could further refine the MG's performance in response to islanding scenarios.

Nevertheless, the overall findings underscore a fundamental characteristic of the algorithm: it prioritizes a comprehensive and exhaustive process, ensuring the pursuit of feasible islanding solutions for all potential event scenarios. This commitment to resilience and robustness in MG network operation defines a critical aspect of the proposed solution method, reinforcing its practicality and adaptability in managing unforeseen challenges and disturbances.

Moving forward, a crucial insight gleaned from the results is the clear economic advantage of layout L1, which consistently demonstrates the lowest cost across both day-ahead scheduling and islanding scenarios when compared to the configurations of L2 and L3. It's worth emphasizing that these cost calculations are meticulously

conducted, accounting for various factors, including system losses such as line losses and transmission losses. The results not only underscore the economic feasibility but also provide a compelling rationale for the integration of networked MGs. This underscores the inherent efficiency and cost-effectiveness of a networked MG infrastructure.

Moreover, when compared with the more straight forward Single Stage MILP approach, the proposed method showed better performance as the number of scenarios increased. Because the level of uncertainty is extremely high in case of natural disasters, it is not possible to guarantee resilience of a system unless it is verified to remain operational in all possible scenarios of that event. This work demonstrates that for such large number of scenarios, the traditional Single Stage MILP approach becomes computationally intractable. On another note, as discussed in section 2.8.2.2, dual of a LP problem with complicating variable structure is another LP problem of complicating constraint structure. Therefore, the decomposition methods like Dantzig Wolf and Bender's can be used interchangeably by finding the dual of the LP problem. However, such is not the case with MILP problems. Dantiz Wolf or Column Generation method is not easily applicable to MILP problems of complicating variable structure. As a result, Bender's Decomposition is the most viable approach for optimal day-ahead scheduling of networked MGs for resilient operation.

5.2 Contributions

A list of the main contributions of this dissertation is presented below:

1. Proposing an Innovative Scheduling Method: The primary objective is to introduce a groundbreaking approach for scheduling multiple MG resources. This method prioritizes resilient operation while simultaneously minimizing operating costs to make MG operation more efficient and dependable.

2. Securing resilient operation under extreme weather events: The proposed approach ensures that MGs can maintain zero generation-load mismatch in numerous potential scenarios resulting from extreme weather events.Therefore, load shedding is

reserved as the last resort.

3. Comparing day-ahead scheduling and resilient operation costs: An essential part of this research is analyzing and comparing the costs associated with traditional day-ahead scheduling and the resilient operation approach for different MG layouts. By quantifying these costs, researchers can demonstrate the advantages and potential savings of networking the MGs in scenarios involving extreme weather events.

4. Handling uncertainties with large number of scenarios and sensitivity analysis: Resiliency in MGs often involves dealing with various uncertainties. This research aims to tackle these uncertainties by employing large number of possible scenarios. Also, the presented sensitivity to generation or load forecasting error allows for a structured exploration of multiple potential outcomes and helps in designing robust strategies.

5. Efficiency Comparison of Optimization Techniques: This research goes a step further by comparing two different optimization techniques: Bender's Decomposition and Single Stage MILP. What makes this study unique is that it evaluates these techniques within a large MG system and across a substantial number of scenarios. This comparison can shed light on the strengths and weaknesses of each method, helping researchers and practitioners choose the most suitable one for their specific applications.

In summary, this research is dedicated to addressing the complex challenges of MG resiliency and efficiency in the context of extreme weather events. It leverages innovative methods, rigorous testing, and comparative analysis to advance the field of MG management.

5.3 Future Work

By venturing into this uncharted territory, the research not only introduces new and intriguing challenges but also opens the door to a plethora of innovative research opportunities. This extension to MG clusters has the potential to drive further ad-

vancements in the field, offering valuable insights and solutions for managing MG islanding scenarios during adverse conditions.

One promising avenue for further enhancing the proposed approach involves integrating considerations for battery degradation costs into the objective function. This could be achieved by obtaining the convexity of the battery degradation model, thus introducing a practical dimension to the model. By incorporating battery degradation costs, the optimization becomes even more robust and versatile, aligning it more closely with real-world applications. This improvement is particularly pertinent in scenarios where battery health and longevity are significant concerns, such as in renewable energy integration projects.

Furthermore, the comparative analysis of the proposed method with the traditional Single Stage MILP approach has already demonstrated its favorable performance in practical applications. However, it would be intriguing to expand the comparison to include an additional single-stage optimization approach mentioned in Section 2.6.1, known as Goal Programming. Such a comparison would yield valuable insights into the relative strengths and weaknesses of these different methodologies, helping to inform the selection of the most suitable approach for specific use cases.

Additionally, this research has taken into account a substantial number of islanding scenarios, which are based on the networked MGs' connection to the main grid. An exciting avenue for further exploration could be the inclusion of scenarios that consider the interconnectivity between neighboring MGs. This extension would provide a more comprehensive view of the resilience and optimization possibilities within a broader grid network, which is increasingly relevant in the context of modern, interconnected energy systems. In conclusion, while the proposed formulation represents a significant breakthrough both in terms of its application and the depth of analysis, it presents an exciting platform for future research endeavors.

REFERENCES

[1] L. Che, X. Zhang, M. Shahidehpour, A. Alabdulwahab, and A. Abusorrah, "Optimal interconnection planning of community microgrids with renewable energy sources," *IEEE Trans. Smart Grid*, vol. 8, pp. 1054–1063, May 2017.

[2] Z. Li, M. Shahidehpour, F. Aminifar, A. Alabdulwahab, and Y. Al-Turki, "Networked microgrids for enhancing the power system resilience," *Proceedings of the IEEE*, vol. 105, no. 7, pp. 1289–1310, Jul 2017.

[3] F. Kamal and B. Chowdhury, "Model predictive control and optimization of networked microgrids," *International Journal of Electrical Power & Energy Systems*, vol. 138, no. 0142-0615, p. 107804, June 2022.

[4] M. S. Q. Zhou, S. B. A. Paaso, A. Alabdulwahab, and A. Abusorrah, "Distributed control and communication strategies in networked microgrids," *IEEE Commun. Surveys Tuts*, vol. 8, pp. 1054–1063, May 2017.

[5] M. Ortiz-Rangel, L. Rueda-Vasquez, C. Duarte-Gualdron, J. Petit, and G. Ordóñez-Plata, "Towards a smart city: Design of a domestic smart grid," in *2015 IEEE PES Innovative Smart Grid Technologies Latin America (ISGT LATAM)*, pp. 863–868, 2015.

[6] A. Y. S. Lam, Y.-W. Leung, and X. Chu, "Electric vehicle charging station placement: Formulation, complexity, and solutions," *IEEE Transactions on Smart Grid*, vol. 5, no. 6, pp. 2846–2856, 2014.

[7] W. V. Torre, N. Bartek, and B. Washom, "The san diego regional experience in developing microgrids, a collaboration between utility and a local university," in *2012 IEEE Power and Energy Society General Meeting*, pp. 1–2, 2012.

[8] R. H. Lasseter, J. H. Eto, B. Schenkman, J. Stevens, H. Vollkommer, D. Klapp, E. Linton, H. Hurtado, and J. Roy, "Certs microgrid laboratory test bed," *IEEE Transactions on Power Delivery*, vol. 26, no. 1, pp. 325–332, 2011.

[9] O. D. E., A. Mehrizi-Sani, A. H. Etemadi, C. A. Cañizares, R. Iravani, M. Kazerani, A. H. Hajimiragha, O. Gomis-Bellmunt, M. Saeedifard, R. Palma-Behnke, G. A. Jiménez-Estévez, and N. D. Hatziargyriou, "Trends in microgrid control," *IEEE Transactions on Smart Grid*, vol. 5, no. 4, pp. 1905–1919, 2014.

[10] K. P. Schneider, F. K. Tuffner, M. A. Elizondo, C.-C. Liu, Y. Xu, S. Backhaus, and D. Ton, "Enabling resiliency operations across multiple microgrids with grid friendly appliance controllers," *IEEE Transactions on Smart Grid*, vol. 9, no. 5, pp. 4755–4764, 2018.

[11] C. F. Weems, S. E. Watts, M. A. Marsee, L. K. Taylor, N. M. Costa, M. F. Cannon, V. G. Carrion, and A. A. Pina, "The psychosocial impact of hurricane katrina: Contextual differences in psychological symptoms, social support, and

discrimination," *IEEE Transactions on Smart Grid*, vol. 45, no. 10, pp. 2295–2306, Oct 2007.

[12] J. L. Corwin and W. T. Miles, "Economic impact of hurricane sandy potential economic activity lost and gained in new jersey and new york," tech. rep., Econ. Stat. Admin., U.S. Dept. Commerce, Washington, DC, USA, Sept 2013.

[13] J. L. Corwin and W. T. Miles, "Impact assessment of the 1977 new york city blackout: Final report," tech. rep., U.S. Dept. Energy, Washington, DC, USA, July 1978.

[14] R. H. Lasseter, "Smart distribution: Coupled microgrids," *Proceedings of the IEEE*, vol. 99, no. 6, pp. 1074–1082, 2011.

[15] A. Pandit, H. Jeong, J. C. Crittenden, and M. Xu, "An infrastructure ecology approach for urban infrastructure sustainability and resiliency," in *2011 IEEE/PES Power Systems Conference and Exposition*, pp. 1–2, 2011.

[16] D. T. Nguyen, Y. Shen, and M. T. Thai, "Detecting critical nodes in interdependent power networks for vulnerability assessment," *IEEE Transactions on Smart Grid*, vol. 4, no. 1, pp. 151–159, 2013.

[17] S. Chanda and A. K. Srivastava, "Defining and enabling resiliency of electric distribution systems with multiple microgrids," *IEEE Transactions on Smart Grid*, vol. 7, no. 6, pp. 2859–2868, 2016.

[18] S. Chanda and A. K. Srivastava, "Quantifying resiliency of smart power distribution systems with distributed energy resources," in *2015 IEEE 24th International Symposium on Industrial Electronics (ISIE)*, pp. 766–771, 2015.

[19] A. Khodaei, "Resiliency-oriented microgrid optimal scheduling," *IEEE Transactions on Smart Grid*, vol. 5, no. 4, pp. 1584–1591, 2014.

[20] S. Zonouz, C. M. Davis, K. R. Davis, R. Berthier, R. B. Bobba, and W. H. Sanders, "Socca: A security-oriented cyber-physical contingency analysis in power infrastructures," *IEEE Transactions on Smart Grid*, vol. 5, no. 1, pp. 3–13, 2014.

[21] A. Arab, A. Khodaei, S. K. Khator, K. Ding, V. A. Emesih, and Z. Han, "Stochastic pre-hurricane restoration planning for electric power systems infrastructure," *IEEE Transactions on Smart Grid*, vol. 6, no. 2, pp. 1046–1054, 2015.

[22] T. Sakaguchi and K. Matsumoto, "Development of a knowledge based system for power system restoration," *IEEE Power Engineering Review*, vol. PER-3, no. 2, pp. 25–26, 1983.

[23] T. Nagata and H. Sasaki, "A multi-agent approach to power system restoration," *IEEE Transactions on Power Systems*, vol. 17, no. 2, pp. 457–462, 2002.

[24] N. Nikmehr and S. Najafi-Ravadanegh, "Probabilistic optimal power dispatch in multi-microgrids using heuristic algorithms," in *2014 Smart Grid Conference (SGC)*, pp. 1–6, 2014.

[25] M. R. Sandgani and S. Sirouspour, "Coordinated optimal dispatch of energy storage in a network of grid-connected microgrids," *IEEE Transactions on Sustainable Energy*, vol. 8, no. 3, pp. 1166–1176, 2017.

[26] A. Ouammi, H. Dagdougui, L. Dessaint, and R. Sacile, "Coordinated model predictive-based power flows control in a cooperative network of smart microgrids," *IEEE Transactions on Smart Grid*, vol. 6, no. 5, pp. 2233–2244, 2015.

[27] Z. Wang, B. Chen, J. Wang, and J. kim, "Decentralized energy management system for networked microgrids in grid-connected and islanded modes," *IEEE Transactions on Smart Grid*, vol. 7, no. 2, pp. 1097–1105, 2016.

[28] P. Tian, X. Xiao, K. Wang, and R. Ding, "A hierarchical energy management system based on hierarchical optimization for microgrid community economic operation," *IEEE Transactions on Smart Grid*, vol. 7, no. 5, pp. 2230–2241, 2016.

[29] L. Che, M. Shahidehpour, A. Alabdulwahab, and Y. Al-Turki, "Hierarchical coordination of a community microgrid with ac and dc microgrids," *IEEE Transactions on Smart Grid*, vol. 6, no. 6, pp. 3042–3051, 2015.

[30] A. Parisio, C. Wiezorek, T. KyntÃ€jÃ€, J. Elo, K. Strunz, and K. H. Johansson, "Cooperative mpc-based energy management for networked microgrids," *IEEE Transactions on Smart Grid*, vol. 8, no. 6, pp. 3066–3074, 2017.

[31] R. Halvgaard, L. Vandenberghe, N. K. Poulsen, H. Madsen, and J. B. JÃžrgensen, "Distributed model predictive control for smart energy systems," *IEEE Transactions on Smart Grid*, vol. 7, no. 3, pp. 1675–1682, 2016.

[32] D. E. Olivares, C. A. Cañizares, and M. Kazerani, "A centralized energy management system for isolated microgrids," *IEEE Transactions on Smart Grid*, vol. 5, no. 4, pp. 1864–1875, 2014.

[33] Z. Wang, B. Chen, J. Wang, and C. Chen, "Networked microgrids for self-healing power systems," *IEEE Transactions on Smart Grid*, vol. 7, no. 1, pp. 310–319, 2016.

[34] A. Khodaei, "Microgrid optimal scheduling with multi-period islanding constraints," *IEEE Transactions on Power Systems*, vol. 29, no. 3, pp. 1383–1392, 2014.

[35] E. Galvan, P. Mandal, and Y. Sang, "Networked microgrids with roof-top solar pv and battery energy storage to improve distribution grids resilience to natural disasters," *Int. J. Electr. Power Energy Syst*, vol. 123, no. 106239, Dec 2020.

[36] A. Hussain, V.-H. Bui, and H.-M. Kim, "Resilience-oriented optimal operation of networked hybrid microgrids," *IEEE Transactions on Smart Grid*, vol. 10, no. 1, pp. 204–215, 2019.

[37] H. Farzin, M. Fotuhi-Firuzabad, and M. Moeini-Aghtaie, "Enhancing power system resilience through hierarchical outage management in multi-microgrids," *IEEE Transactions on Smart Grid*, vol. 7, no. 6, pp. 2869–2879, 2016.

[38] J. N. Brass, S. Carley, L. M. MacLean, and E. Baldwin, "Power for development: A review of distributed generation projects in the developing world," *Society for Industrial and Applied Mathematics*, vol. 37, pp. 107–136, 2012.

[39] T. Ackermann, G. Andersson, and L. Söder, "Distributed generation: a definition," *Electric Power Systems Research*, vol. 57, no. 3, pp. 195–204, 2001.

[40] S. Carley, "Distributed generation: An empirical analysis of primary motivators," *Energy Policy*, vol. 37, no. 5, pp. 1648–1659, 2009.

[41] E. Adkins, S. Eapen, F. Kaluwile, G. Nair, and V. Modi, "Off-grid energy services for the poor: Introducing led lighting in the millennium villages project in malawi," *Energy Policy*, vol. 38, no. 2, pp. 1087–1097, 2010.

[42] Z. Contreras, "Planning paths for the electrification of small villages using decentralised generation: Experience from senegal," *International Journal of Energy Sector Management*, vol. 2, no. 1, pp. 118–138, 2008.

[43] A. S. A. Diniz, L. V. M. Neto, C. F. Camara, P. Morais, C. V. Cabral, D. O. Filho, R. F. Ravinetti, E. D. França, D. A. Cassini, M. E. Souza, J. H. Santos, and M. Amorim, "Review of the photovoltaic energy program in the state of minas gerais, brazil," *Renewable and Sustainable Energy Reviews*, vol. 15, no. 6, pp. 2696–2706, 2011.

[44] B. E. Advisor, "Small scale distributed generation technologies," tech. rep., Orlando Utilities Commission, 2019.

[45] R. Lasseter, A. Akhil, C. Marnay, J. Stephens, J. Dagle, R. Guttromsom, A. S. Meliopoulous, R. Yinger, and J. Eto, "Integration of distributed energy resources. the certs microgrid concept," tech. rep., U.S. Department of Energy Office of Scientific and Technical Information, 4 2002.

[46] W. Su and J. Wang, "Energy management systems in microgrid operations," *The Electricity Journal*, vol. 25, no. 8, pp. 45–60, 2012.

[47] R. Georgious, R. Refaat, J. Garcia, and A. A. Daoud, "Review on energy storage systems in microgrids," *Electronics*, vol. 10, no. 17, 2021.

[48] S. Atcitty, "An introduction to microgrids and energy storage." Available at https://www.energy.gov/sites/default/files/2022-08/$3_{S}tan - Atcitty_{M}icrogrids - and - Energy - Storage.pdf$(10/14/2023).

[49] X. Luo, J. Wang, M. Dooner, and J. Clarke, "Overview of current development in electrical energy storage technologies and the application potential in power system operation," *Applied Energy*, vol. 137, pp. 511–536, 2015.

[50] S. Sabihuddin, A. E. Kiprakis, and M. Mueller, "A numerical and graphical review of energy storage technologies," *Energies*, vol. 8, no. 1, pp. 172–216, 2015.

[51] E. Bullich-Massagué, F. Díaz-González, M. Aragüés-Peñalba, and A. S. F. Girbau-Llistuella, P. Olivella-Rosell, "Microgrid clustering architectures," *Applied Energy*, vol. 212, pp. 340–361, 2018.

[52] N. J. Gil and J. A. P. Lopes, "Hierarchical frequency control scheme for islanded multi-microgrids operation," in *2007 IEEE Lausanne Power Tech*, July 2007.

[53] A. Madureira and J. P. Lopes, "Coordinated voltage support in distribution networks with distributed generation and microgrids," *IET Renewable Power Generation*, vol. 3, pp. 439–454, Dec 2009.

[54] A. Madureira, J. Pereira, N. Gil, J. P. Lopes, G. Korres, and N. Hatziargyriou, "Advanced control and management functionalities for multi-microgrids," *European Transactions on Electrical Power*, vol. 21, no. 2, pp. 1159–1177, Mar 2011.

[55] F. Resende, N. Gil, and J. P. Lopesl, "Service restoration on distribution systems using multi-microgrids," *European Transactions on Electrical Power*, vol. 21, no. 2, pp. 1327–1342, Mar 2011.

[56] J.-M. Rodriguez-Bernuz, E. Prieto-Araujo, F. Girbau-Llistuella, A. Sumper, R. Villafafila-Robles, and J.-A. Vidal-Clos, "Experimental validation of a single phase intelligent power router," *Sustainable Energy, Grids and Networks*, vol. 4, pp. 1–15, Dec 2015.

[57] M. Goyal and A. Ghosh, "Microgrids interconnection to support mutually during any contingency," *Sustainable Energy, Grids and Networks*, vol. 6, pp. 100–108, Jun 2016.

[58] S. Bala and G. Venkataramanan, "Microgrids interconnection to support mutually during any contingency," in *IEEE Energy Conversion Congress and Exposition*, pp. 3006–3013, Sep 2009.

[59] I. Nutkani, P. Loh, and F. Blaabjerg, "Power flow control of intertied ac microgrids," *IET Power Elect*, vol. 6, no. 7, pp. 1329–1338, Aug 2013.

[60] X. Zhou, L. Zhou, Y. Chen, J. M. Guerrero, A. Luo, W. Wu, and L. Yang, "A microgrid cluster structure and its autonomous coordination control strategy," *International Journal of Electrical Power & Energy Systems*, vol. 100, pp. 69–80, 2018.

[61] L. Meng, Q. Shafiee, G. F. Trecate, H. Karimi, D. Fulwani, X. Lu, and J. M. Guerrero, "Review on control of dc microgrids and multiple microgrid clusters," *IEEE Journal of Emerging and Selected Topics in Power Electronics*, vol. 5, no. 3, pp. 928–948, 2017.

[62] W. Zhang, Z. D. Y. Xu, and K. P. Wong, "Robust security constrained-optimal power flow using multiple microgrids for corrective control of power systems under uncertainty," *IEEE Transactions on Industrial Informatics*, vol. 13, no. 4, pp. 1704–1713, Aug 2017.

[63] F. Shahnia, S. Bourbour, and A. Ghosh, "Coupling neighboring microgrids for overload management based on dynamic multicriteria decision-making," *IEEE Transactions on Smart Grid*, vol. 8, no. 2, pp. 969–983, Mar 2017.

[64] A. Arefi and F. Shahnia, "Tertiary controller-based optimal voltage and frequency management technique for multi-microgrid systems of large remote towns," *IEEE Transactions on Smart Grid*, vol. 9, no. 6, pp. 5962–5974, Nov 2018.

[65] F. Shahnia and A. Arefi, "Defining the suitable adjacent microgrids to form a temporary system of coupled microgrids," in *IEEE Region 10 Conference (TENCON)*, pp. 1216–1219, Nov 2016.

[66] M. S. Rahman, M. J. Hossain, F. H. M. Rafi, and J. Lu, "A multi-purpose interlinking converter control for multiple hybrid ac/dc microgrid operations," in *IEEE Innovative Smart Grid Technologies - Asia (ISGT-Asia)*, pp. 221–226, 2016.

[67] H. Zhang, J. Zhou, Q. Sun, J. M. Guerrero, and D. Ma *IEEE Transactions on Smart Grid*, vol. 8, no. 2, pp. 557–571, Mar 2017.

[68] P. Wu, W. Huang, N. Tai, and S. Liang, "A novel design of architecture and control for multiple microgrids with hybrid ac/dc connection," *Applied Energy*, vol. 210, pp. 1002–1016, Jan 2018.

[69] C. Jin, P. C. Loh, P. Wang, Y. Mi, and F. Blaabjerg, "Autonomous operation of hybrid ac-dc microgrids," in *IEEE International Conference on Sustainable Energy Technologies*, pp. 1–7, 2010.

[70] L. Che, M. Shahidehpour, A. Alabdulwahab, and Y. Al-Turki, "Hierarchical coordination of a community microgrid with ac and dc microgrids," *IEEE Trans. on Smart Grid*, vol. vol. 6, no. 6, pp. 3042–3051, 2015.

[71] P. C. Loh, D. Li, Y. K. Chai, and F. Blaabjerg, "Autonomous control of interlinking converter with energy storage in hybrid ac-dc microgrid," *IEEE Transactions on Industry Applications*, vol. 49, no. 3, pp. 1374–1382, May-June 2013.

[72] P. Wang, C. Jin, D. Zhu, Y. Tang, P. C. Loh, and F. H. Choo, "Distributed control for autonomous operation of a three-port ac/dc/ds hybrid microgrid," *IEEE Transactions on Industrial Electronics*, vol. 62, no. 2, pp. 1279–1290, Feb 2015.

[73] N. Eghtedarpour and E. Farjah, "Power control and management in a hybrid ac/dc microgrid," *IEEE Transactions on Smart Grid*, vol. 5, no. 3, pp. 1494–1505, May 2014.

[74] M. Hamidieh and M. Ghassemi, "Microgrids and resilience: A review," *IEEE Access*, vol. 10, pp. 106059–106080, 2022.

[75] What is a Natural Hazard? | GEOG 30N: Environment and Society in a Changing World. Accessed: Oct 14, 2023. [Online]. Available: https://www.e-education.psu.edu/geog30/node/378.

[76] "The world's second largest blackout | rhodium group." https://rhg.com/research/puerto-rico-hurricane-maria-worlds-second-largest-blackout/. Accessed: Oct 14, 2023.

[77] "Combating the climate crisis | department of energy.." https://www.energy.gov/combating-climate-crisis. Accessed: Oct 14, 2023.

[78] N. Makhoul and S. Argyroudis, "Tools for resilience assessment: Developments, limitations and future needs," 06 2019.

[79] A. Khodaei, "Resiliency-oriented microgrid optimal scheduling," *IEEE Transactions on Smart Grid*, vol. 5, no. 4, pp. 1584–1591, 2014.

[80] A. Gholami, T. Shekari, F. Aminifar, and M. Shahidehpour, "Microgrid scheduling with uncertainty: The quest for resilience," *IEEE Transactions on Smart Grid*, vol. 7, no. 6, pp. 2849–2858, 2016.

[81] G. Liu, T. B. Ollis, Y. Zhang, T. Jiang, and K. Tomsovic, "Robust microgrid scheduling with resiliency considerations," *IEEE Access*, vol. 8, pp. 153169–153182, 2020.

[82] L. Tightiz and H. Yang, "Resilience microgrid as power system integrity protection scheme element with reinforcement learning based management," *IEEE Access*, vol. 9, pp. 83963–83975, 2021.

[83] M. Starke, B. Xiao, and K. Tomsovic, "Robust optimisation-based microgrid scheduling with islanding constraints," *IET Generation Transmission and Distribution*, vol. 11, no. 7, pp. 1820–1828, 2017.

[84] H. Shahinzadeh, S. Nikolovski, J. Moradi, and R. Bayindir, "A resilience-oriented decision-making model for the operation of smart microgrids subject to techno-economic and security objectives," in *2021 9th International Conference on Smart Grid (icSmartGrid)*, pp. 226–230, 2021.

[85] D. Gutierrez-Rojas, A. Mashlakov, C. Brester, H. Niska, M. Kolehmainen, A. Narayanan, S. Honkapuro, and P. H. J. Nardelli, "Weather-driven predictive control of a battery storage for improved microgrid resilience," *IEEE Access*, vol. 9, pp. 163108–163121, 2021.

[86] Z. Wang, B. Chen, J. Wang, and C. Chen, "Networked microgrids for self-healing power systems," *IEEE Transactions on Smart Grid*, vol. 7, no. 1, pp. 310–319, 2016.

[87] S. Teimourzadeh, O. B. Tor, M. E. Cebeci, A. Bara, and S. V. Oprea, "A three-stage approach for resilience-constrained scheduling of networked microgrids," *Journal of Modern Power Systems and Clean Energy*, vol. 7, no. 4, pp. 705–715, 2019.

[88] M. E. Parast, M. H. Nazari, and S. H. Hosseinian, "Resilience improvement of distribution networks using a two-stage stochastic multi-objective programming via microgrids optimal performance," *IEEE Access*, vol. 9, pp. 102930–102952, 2021.

[89] Y. Wang, A. O. Rousis, and G. Strbac, "A three-level planning model for optimal sizing of networked microgrids considering a trade-off between resilience and cost," *IEEE Transactions on Power Systems*, vol. 36, no. 6, pp. 5657–5669, 2021.

[90] M. S. Alam and S. A. Arefifar, "Iot-based mobile energy storage operation in multi-mg power distribution systems to enhance system resiliency," *Energies*, vol. 15, no. 1, 2022.

[91] R. Nourollahi, P. Salyani, K. Zare, and R. Razzaghi, "A two-stage hybrid robust-stochastic day-ahead scheduling of transactive microgrids considering the possibility of main grid disconnection," *International Journal of Electrical Power & Energy Systems*, vol. 136, p. 107701, 2022.

[92] H. S. Fesagandis, M. Jalali, K. Zare, M. Abapour, and H. Karimipour, "Resilient scheduling of networked microgrids against real-time failures," *IEEE Access*, vol. 9, pp. 21443–21456, 2021.

[93] O. de Weck, 'Multiobjective Optimization: History and Promise', https://api.semanticscholar.org/CorpusID:260895977.

[94] H. A. Qahtani, A. El-Hefnawy, M. M. El-Ashram, and A. Fayomi1, "A goal programming approach to multichoice multiobjective stochastic transportation problems with extreme value distribution," *Advances in Operations Research*, vol. 2019, 2019.

[95] J. P. Ignizio, "A review of goal programming: A tool for multiobjective analysis," *IEEE Access*, vol. 29, no. 11, pp. 1109–1119, 1978.

[96] G. P. McCORMICK, *Computability of Global Solutions to Factorable Non convex Programs: Part I - Convex Underestimating Problems*. North-Holland Publishing Company, 1976.

[97] S. Urban, 'McCormick Envelopes', Cornell University, SYSEN 5800, Fall 2021, https://optimization.cbe.cornell.edu/index.php?title=McCormick_envelopes,.

[98] A. Schrijver, *Theory of Linear and Integer Programming*. John Wiley & Sons Inc., 1986.

[99] M. Guignard-Spielberg and K.Spielberg, *Integer Programming: State of the Art and Recent Advances*, ch. 139. Springer,, 2005.

[100] M. Ju/"nger, T. Liebling, D. Naddef, G. Nemhauser, W. Pulleyblank, G. Reinelt, G. Rinaldi, and L. Wolsey, *50 Years of IntegerProgramming 1958-2008: From the Early Years to the State-of-the-Art*. Springer-Verlag, 2010.

[101] J. Lee, "A celebration of 50 years of integer programming," *Optima*, vol. 76, pp. 10–14, 2008.

[102] IBM ILOG, CPLEX High-Performance Mathematical Programming Engine, http://www.ibm.com/software/integration/optimization/cplex/.

[103] Gurobi Optimization, The Gurobi Optimizer, available online from http://www.gurobi.com.

[104] Zuse Institute Berlin, SCIP: Solving Constraint Integer Programs, http://scip.zib.de/.

[105] T. Achterberg, *Constraint Integer Programming*. PhD thesis, TU, Berlin, 2007.

[106] T. Achterberg, "Scip: Solving constraint integer programs," *Mathematical Programming Computation*, vol. 1, pp. 1–41, 2009.

[107] R. E. Bixby, M. Fenelon, Z. Gu, E. E. Rothberg, and R. Wunderling, "Mip: Theory and practice - closing the gap," in *System Modelling and Optimization*, 1999.

[108] R. Bixby, M. Fenelon, Z. Gu, E. Rothberg, and R. Wunderling, *Mixed-Integer Programming: A Progress Report*, pp. 309–324. 01 2004.

[109] R. Bixby and E. Rothberg, "Progress in computational mixed integer programming: A look back from the other side of the tipping point," *Annals of Operations Research*, vol. 149, pp. 37–41, 2007.

[110] E. L. Johnson, G. L. Nemhauser, and M. W. Savelsbergh, "Progress in linear programming-based algorithms for integer programming: An exposition," *INFORMS Journal on Computing*, vol. 2, pp. 2–23, 2000.

[111] A. Lodi, *Mixed Integer Programming Computation*, pp. 619–645. Berlin, Heidelberg: Springer Berlin Heidelberg, 2010.

[112] G. B. Dantzig, *Discrete-Variable Extremum Problems*, ch. 5, pp. 266–277. No. 2, Informs, 1957.

[113] G. B. Dantzig, "On the significance of solving linear programming problems with some integer variables," *Econometrica*, vol. 28, no. 1, pp. 30–44, 1960.

[114] J. P. Vielma, "Mixed integer linear programming formulation techniques," *Society for Industrial and Applied Mathematics*, vol. 57, no. 1, pp. 3–57, 2015.

[115] C. Lim, *Wiley encyclopedia of operations research and management science*, ch. Relationship among Benders, Dantzig-Wolfe, and Lagrangian optimization. John Wiley & Sons, 2010.

[116] Constraints and duality, CMU School of Computer Science, https://www.cs.cmu.edu/ aarti/Class/10701$_{S}pring21/Lecs/duality.pdf$.

[117] A. J. Conejo, E. Castillo, R. Mínguez, and R. García-Bertrand, *Decomposition Techniques in Mathematical Programming - Engineering and Science Applications*. Springer, 2006.

[118] 'Generator Cost Per kWh: Diesel, Propane, Natural Gas, Gasoline,' 2023. [Online]. Available: https://learnmetrics.com/generator-cost-per-kwh-diesel-propane-natural-gas-gasoline [Accessed: April 29, 2023].

[119] U.S. Department of Energy, 'Hydrogen Shot,' 2021. Available: https://www.energy.gov/eere/fuelcells/hydrogen-shot [Accessed: April 29, 2023].

[120] 'Economics,' Available: https://www.sgh2energy.com/economics [Accessed: April 29, 2023].

[121] Y. Shi, B. Xu, Y. Tan, and B. Zhang, "A convex cycle-based degradation model for battery energy storage planning and operation," in *2018 Annual American Control Conference (ACC)*, 2018.

[122] A. Millner, "Modeling lithium ion battery degradation in electric vehicles," in *2010 IEEE Conference on Innovative Technologies for an Efficient and Reliable Electricity Supply*, pp. 349–356, 2010.

APPENDIX A: Feeder Data

A.1 Modified IEEE 123-bus Test Feeder

Table A.1: Line parameters for modified IEEE 123-bus feeder

Line No.	From Node	To Node	Length (ft)	Capacity (kVA)	Line Type	Config.
1	1	2	175	960	Non-switchable	10
2	1	3	250	960	Non-switchable	11
3	1	7	300	2200	Switchable	1
4	3	4	200	960	Non-switchable	11
5	3	5	325	960	Non-switchable	11
6	5	6	250	960	Non-switchable	11
7	7	8	200	2200	Non-switchable	1
8	8	12	225	960	Non-switchable	10
9	8	9	225	960	Non-switchable	9
10	8	13	300	2200	Non-switchable	1
11	9	14	425	960	Non-switchable	9
12	13	34	150	960	Non-switchable	11
13	13	18	825	2200	Switchable	2
14	13	152	10	3700	Switchable	13
15	14	11	250	960	Non-switchable	9
16	14	10	250	960	Non-switchable	9
17	15	16	375	960	Non-switchable	11
18	15	17	350	960	Non-switchable	11
19	18	19	250	960	Non-switchable	9
20	18	21	300	2200	Non-switchable	2
21	18	135	10	3700	Switchable	13
22	19	20	325	960	Non-switchable	9
23	21	22	525	960	Non-switchable	10
24	21	23	250	2200	Non-switchable	2
25	23	24	550	960	Non-switchable	11
26	23	25	275	2200	Switchable	2
27	25	26	350	2200	Non-switchable	7
28	25	28	200	2200	Non-switchable	2
29	26	27	275	2200	Non-switchable	7
30	26	31	225	960	Non-switchable	11
31	27	33	500	960	Non-switchable	9
32	28	29	300	2200	Non-switchable	2
33	29	30	350	2200	Non-switchable	2
34	30	250	200	2200	Non-switchable	2
35	31	32	300	960	Non-switchable	11

Line No.	From Node	To Node	Length (ft)	Capacity (kVA)	Line Type	Config.
36	34	15	100	960	Non-switchable	11
37	35	36	650	2200	Non-switchable	8
38	35	40	250	2200	Non-switchable	1
39	36	37	300	960	Non-switchable	9
40	36	38	250	960	Non-switchable	10
41	38	39	325	960	Non-switchable	10
42	40	41	325	960	Non-switchable	11
43	40	42	250	2200	Non-switchable	1
44	42	43	500	960	Non-switchable	10
45	42	44	200	2200	Non-switchable	1
46	44	45	200	960	Non-switchable	9
47	44	47	250	2200	Non-switchable	1
48	45	46	300	960	Non-switchable	9
49	47	48	150	2200	Non-switchable	4
50	47	49	250	2200	Non-switchable	4
51	49	50	250	2200	Non-switchable	4
52	50	51	250	2200	Non-switchable	4
53	51	151	500	2200	Non-switchable	13
54	52	53	200	2200	Non-switchable	1
55	53	54	125	2200	Non-switchable	1
56	54	55	275	2200	Non-switchable	1
57	54	57	350	2200	Non-switchable	3
58	54	94	10	3700	Switchable	13
59	55	56	275	2200	Non-switchable	1
60	57	58	250	960	Non-switchable	10
61	57	60	750	2200	Non-switchable	3
62	58	59	250	960	Non-switchable	10
63	60	61	550	2200	Non-switchable	5
64	60	62	250	730	Non-switchable	12
65	60	160	10	3700	Switchable	13
66	61	610	10	150	Non-switchable	13
67	62	63	175	730	Non-switchable	12
68	63	64	350	730	Non-switchable	12
69	64	65	425	730	Non-switchable	12
70	65	66	325	730	Non-switchable	12
71	67	68	200	960	Non-switchable	9
72	67	72	275	2200	Non-switchable	3
73	67	97	250	2200	Non-switchable	3
74	68	69	275	960	Non-switchable	9
75	69	70	325	960	Non-switchable	9
76	70	71	275	960	Non-switchable	9
77	72	73	275	960	Non-switchable	11

Line No.	From Node	To Node	Length (ft)	Capacity (kVA)	Line Type	Config.
78	72	76	200	2200	Non-switchable	3
79	73	74	350	960	Non-switchable	11
80	74	75	400	960	Non-switchable	11
81	76	77	400	2200	Switchable	6
82	76	86	700	2200	Non-switchable	3
83	77	78	100	2200	Non-switchable	6
84	78	79	225	2200	Non-switchable	6
85	78	80	475	2200	Non-switchable	6
86	80	81	475	2200	Non-switchable	6
87	81	82	250	2200	Non-switchable	6
88	81	84	675	960	Non-switchable	11
89	82	83	250	2200	Non-switchable	6
90	84	85	475	960	Non-switchable	11
91	86	87	450	2200	Non-switchable	6
92	87	88	175	960	Non-switchable	9
93	87	89	275	2200	Switchable	6
94	89	90	225	960	Non-switchable	10
95	89	91	225	2200	Non-switchable	6
96	91	92	300	960	Non-switchable	11
97	91	93	225	2200	Non-switchable	6
98	93	94	275	960	Non-switchable	9
99	93	95	300	2200	Non-switchable	6
100	95	96	200	960	Non-switchable	10
101	97	98	275	2200	Non-switchable	3
102	97	197	10	3700	Switchable	13
103	98	99	550	2200	Non-switchable	3
104	99	100	300	2200	Non-switchable	3
105	100	450	800	2200	Non-switchable	3
106	101	102	225	960	Non-switchable	11
107	101	105	275	2200	Non-switchable	3
108	102	103	325	960	Non-switchable	11
109	103	104	700	960	Non-switchable	11
110	105	106	225	960	Non-switchable	10
111	105	108	325	2200	Non-switchable	3
112	106	107	575	960	Non-switchable	10
113	108	109	450	960	Non-switchable	9
114	108	300	1000	2200	Non-switchable	3
115	109	110	300	960	Non-switchable	9
116	110	111	575	960	Non-switchable	9
117	110	112	125	960	Non-switchable	9
118	112	113	525	960	Non-switchable	9
119	113	114	325	960	Non-switchable	9

Line No.	From Node	To Node	Length (ft)	Capacity (kVA)	Line Type	Config.
120	135	35	375	2200	Non-switchable	4
121	149	1	400	2200	Non-switchable	1
122	150	149	10	3700	Switchable	13
123	151	300	10	3700	Switchable	13
124	152	52	400	2200	Non-switchable	1
125	160	67	350	2200	Non-switchable	6
126	197	101	250	2200	Non-switchable	3

Table A.2: Line impedances for modified IEEE 123-bus feeder

Config.	Resistance (Ohms/mi)	Reactance (Ohms/mi)
1	0.4619	1.0638
2	0.4619	1.0638
3	0.4619	1.0638
4	0.4619	1.0638
5	0.4619	1.0638
6	0.4619	1.0638
7	0.4576	1.0780
8	0.4596	1.0716
9	1.3292	1.3475
10	1.3292	1.3475
11	1.3292	1.3475
12	1.5249	0.7401
13	0.0100	0.0100

Table A.3: Load parameters for modified IEEE 123-bus feeder

Load Name	P (kW)	Q (kVar)	Load Name	P (kW)	Q (kVar)	Load Name	P (kW)	Q (kVar)
L1	15	5	L43	15	5	L79	15	5
L2	5	5	L45	5	5	L80	15	5
L4	15	5	L46	5	5	L82	15	5
L5	5	5	L47	35	25	L83	5	5
L6	15	5	L48	70	50	L84	5	5
L7	5	5	L49	45	30	L85	15	5
L9	15	5	L50	15	5	L86	5	5
L10	5	5	L51	5	5	L87	15	5
L11	15	5	L52	15	5	L88	15	5
L12	5	5	L53	15	5	L90	15	5

Load Name	P (kW)	Q (kVar)	Load Name	P (kW)	Q (kVar)	Load Name	P (kW)	Q (kVar)
L16	15	5	L55	5	5	L92	15	5
L17	5	5	L56	5	5	L94	15	5
L19	15	5	L58	5	5	L95	5	5
L20	15	5	L59	5	5	L96	5	5
L22	15	5	L60	5	5	L98	15	5
L24	15	5	L62	15	5	L99	15	5
L28	15	5	L63	15	5	L100	15	5
L29	15	5	L64	25	10	L102	5	5
L30	15	5	L65	45	35	L103	15	5
L31	5	5	L66	25	10	L104	15	5
L32	5	5	L68	5	5	L106	15	5
L33	15	5	L69	15	5	L107	15	5
L34	15	5	L70	5	5	L109	15	5
L35	15	5	L71	15	5	L111	5	5
L37	15	5	L73	15	5	L112	5	5
L38	5	5	L74	15	5	L113	15	5
L39	5	5	L75	15	5	L114	5	5
L41	5	5	L76	80	60			
L42	5	5	L77	15	5			

Table A.4: Capacitor data for modified IEEE 123-bus feeder

Node	kVar
83	180
88	15
90	15
92	15

Table A.5: Transformer and regulator data for modified IEEE 123-bus feeder

	kVA	kV-high	kV-low	Tap Position
Substation	5000	115	4.16	–
XFM-1	150	4.16	0.48	–
RG 150-149	–	4.16	4.16	-7
RG 9-14	–	4.16	4.16	1
RG 25-26	–	4.16	4.16	1
RG 160-67	–	4.16	4.16	-4